Transport in a disordered quantum dot connected to one dimensional leads.

Transporteigenschaften eines ungeordneten Quantenpunkts angeschlossen an eindimensionale Leiter.

Stefan Wichmann

Munich 2013

Transport in a disordered quantum dot connected to one dimensional leads.

Transporteigenschaften eines ungeordneten Quantenpunkts angeschlossen an eindimensionale Leiter.

Bachelor-Thesis

at the

Ludwig–Maximilians–University

submitted by

Stefan Wichmann

(Matr. Nr.: 10397423)

born on the 05.09.1990 in D-92637 Weiden

supervised by

Prof. Dr. Jan von Delft

and
Dr. Oleg Yevtushenko

Munich, the December 20, 2013

Evaluator: Prof. Dr. Jan von Delft

Day of oral exam: _____

Contents

1. Introduction **1**

2. The emergence of the broad energy levels **13**

3. The random matrix approach **14**
3.1. The total Hamiltonian 14
3.2. Impact of the leads on the dot 15

4. Description of the QPC **18**
4.1. Deriving the S-matrix for the whole system 18
4.2. Finding the scattering matrix of the QPC 20

5. Numerical study of the effective Hamiltonian **23**
5.1. Basic equations 23
5.2. Results of the calculations 24
5.3. Comparing the results to a constant δ model 26

6. Alternative description of the QPC **30**
6.1. Composing S_c from two scatterers 30
6.2. How to express $\tilde{W}$ in terms of $r_{L,R}$ 33

7. Conclusion **34**

A. Derivation of equation (4.21) **35**

B. Code for the random matrix Hamiltonian **37**

C. Code for the constant level spacing Hamiltonian **39**

Bibliography **40**

Acknowledgements **41**

Statutory Declaration **42**

1. Introduction

As smaller and smaller electric circuits can be manufactored by so called nanofabrication [1], physics in systems of mesoscopic lengthscale plays an important role in state of the art experiments. In the mesoscopic regime, which is between the microscopic and the macroscopic ones, objects are small enough, so quantum mechanic behaviour emerges, but big enough, so that a statistical description is also possible. The dimensionless conductance $g = \frac{E_{Th}}{\Delta}$ of such systems should be large, $g \gg 1$, so that the following descriptions are valid. This is equivalent to the Thouless energy $E_{Th} = \frac{\hbar}{\tau_D}$ being much bigger than the average level spacing Δ, which also means that the time τ_D an electron needs to traverse the system is very small. In some samples, the mean free path of an electron can be comparable to the system size. Such systems no longer self-average a quantity like the conductance G. It becomes highly sample dependent, whereby G loses its meaning. At temperatures below the Thouless energy, universal behaviour for G can be observed again. It can be quantized at $T < T_{Th}$ in quantums of $G_Q = \frac{2e^2}{h}$, called the conductance quantum, with e being the elementary charge and h being the Planck constant [2]. In Figure 1.1 experimental setups for investigation of physics on the mesoscopic length scale are presented.

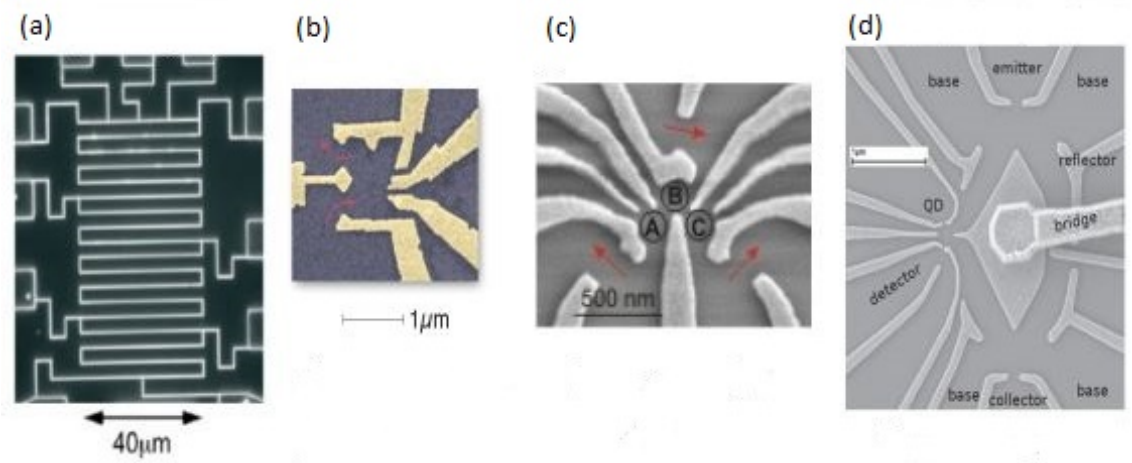

Figure 1.1.: (a) One dimensional wires. (b) A single quantum dot. (c) Three quantum dots A, B and C. (d) A quantum dot in an Aharonov-Bohm ring. The pictures have been copied from [3].

The brighter parts in Figure 1.1 are the gate leads, which are on top of an insulating layer and can be charged. Below the insulator there is the conduction material, which

is thin enough to confine electron movement in one direction. If the conductance of this material is high, as stated before, the electrons inside can be described by a two dimensional electron gas. The electric field of the charged gate leads enter into the material below and the electron gas feels the electric field as a repulsive potential. This potential confines the electrons to certain areas, which define the shape of the system [2]. This mechanism is sketched in Figure 1.2. At this point it is clear, that the microscopic shape of such systems is hard to control and is often not known in experimental setups. Fortunately, the microscopic details are not necessarily needed, as explained later.

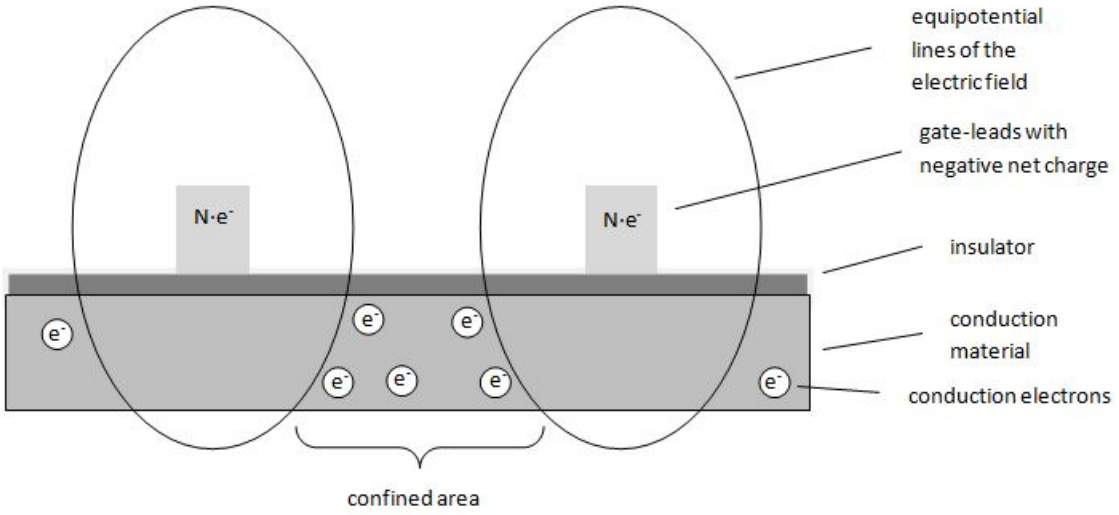

Figure 1.2.: A schematic cross section of the experimental setups in Figure 1.1.

Elements, which are encountered frequently in such systems, are quantum dots (QD) and one dimensional leads. A QD is a cavity like structure, which spacially confines electrons inside. The further description of these objects follow mainly [2] and [3]. A confinement of electrons to the size of QDs leads to discrete energy levels ε_j^0. Electrons can enter and leave the dot via attached leads if they are connected to electron reservoirs. The more electrons are in the dot, the more energy is needed for another electron to hop onto the dot, not only because the lower energy levels are filled up and a single particle level spacing $\delta_j := \varepsilon_{j+1}^0 - \varepsilon_j^0$ has to be overcome, but also because the electron repulsion due to Coulomb interaction has to be compensated by the energy ΔE_N, depending on the number of electrons N already in the dot. One can manipulate the number of electrons by attaching at least one lead to the dot and applying a gate voltage V_g, which shifts all the energy levels of the dot. Electrons can hop into or out of the dot, when the energies of the states ψ_n and ψ_{n+1}, where the index denotes the number of electrons on the dot, is equal. This is equal to the energy difference $\Delta E^{(n)} = 0$ and can be archieved by tuning the gate voltage. The energy difference can be determined from the Hamiltonian of the QD. Further electron-electron interactions to the charging energy will be neglected:

$$\hat{H}_{dot} = \sum_j \varepsilon_j \hat{n}_j + E_c \hat{n}^2 \quad .$$

The first part of the Hamiltonian describes the discretete energy levels, that appear due to the confinement of the electrons, ε_j are the energies of the single particle levels and $\hat{n}_j$ the respective electron number operators with the two eigenvalues 0 or 1 for spinless electrons. The second part is the charging energy of a capacitor, $E_c = \frac{e^2}{2C}$ is the charging energy, with C being the capacity of the dot, and $\hat{n} = \sum_j \hat{n}_j$ is the total electron number operator. $\Delta E^{(n)}$ can be defined as the difference of the expectation values of $\hat{H}_{dot}$ corresponding to the two states ψ_n and ψ_{n+1}. Assuming that the lowest energy levels of the QD are filled, the difference reads:

$$\begin{aligned} \Delta E^{(n)} &= \langle \psi_{n+1} | \hat{H}_{dot} | \psi_{n+1} \rangle - \langle \psi_n | \hat{H}_{dot} | \psi_n \rangle = \\ &= \sum_{j=1}^{n+1} \varepsilon_j + E_c (n+1)^2 - \sum_{j=1}^{n} \varepsilon_j - E_c n^2 = \varepsilon^0_{n+1} - V_g + E_c(2n+1) \\ &\Rightarrow \Delta E^{(n)} = 0 \text{ if } V_g(n) = \varepsilon^0_{n+1} + E_c(2n+1) \end{aligned} \tag{1.1}$$

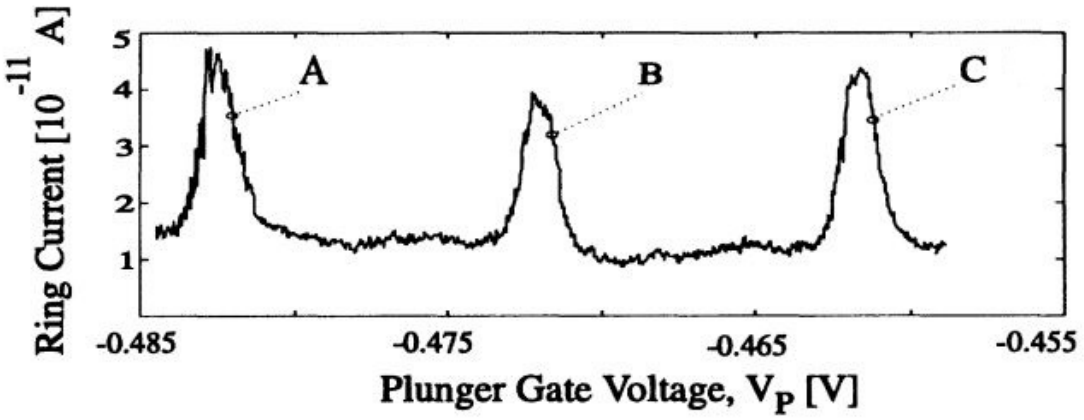

Figure 1.3.: Three CB peaks with CB valleys in between. The picture was taken from [4].

At these values of V_g, an electron can move into the dot and the conductance of the whole system has a peak, which is called a Coulomb-blockade (CB) peak. Figure 1.3 shows experimental data from [4] for the current through an Aharonov-Bohm ring containing a QD. The structure of the Aharonov-Bohm ring will be described later. The data reveals the typical CB peak behaviour as described before. The region between two peaks is called the CB valley. It can be estimated from (1.1) as $\Delta V_{g,n} = V_g(n) - V_g(n-1) = \delta_n + 2E_c$. For systems consisting of many atoms $\delta_j \ll E_c$ holds, so the width of CB valleys is almost constant, equal to $2E_c$.

By attaching two leads to the dot and applying a voltage bias between them,

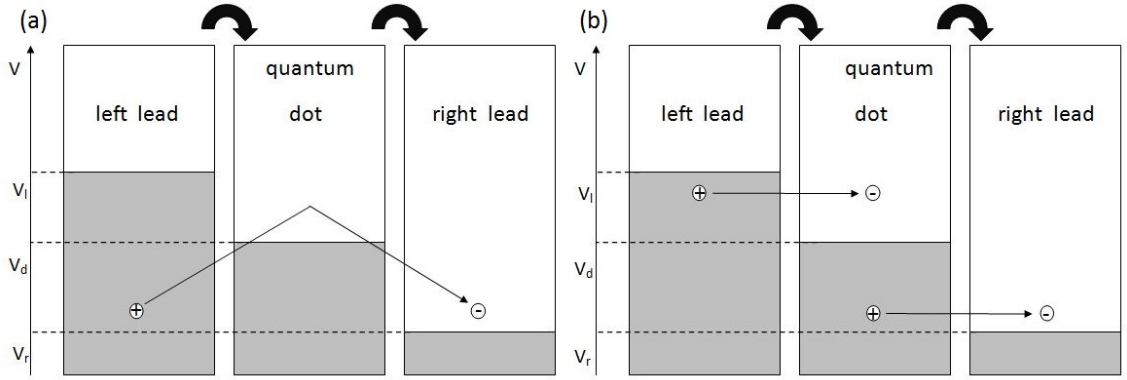

Figure 1.4.: The two possible cotunneling processes. (a) Elastic cotunneling: an electron from the left lead hops into a virtual state on the dot and off to the right lead in one move. The initial and final state have the same energy while the virtual state can have higher energy. In the end there is one hole left in the left lead. (b) Inelastic cotunneling: an elctron from the left lead hops on the dot and another electron from the dot hops off to the right lead in one move. In the end there are two holes, one in the left lead and one on the dot and one extra electron in the dot. The pictues were taken form [3].

electron transport can be realized through the dot. Usually only the lowest empty energy level contributes to electron transport. There are two transport regimes in such a system. One is called the single electron transfer, since in this regime the electrons move one after another and every electron motion to or from the dot is energetically possible ($\Delta E < 0$). The other possible regime is the cotunneling regime, in which electron movements occur simultaneously. This process is sketched in Figure 1.4. It is energetically possible, but will be neglect in this thesis, since they are second order processes. In an ideal system, electron transmission occours only at the gate voltage $V_g(n)$, as described above. But in a real system the coupling of the leads to the dot can be non-trivial, for example, electrons coming from the lead can be coupled to excited states inside the dot and not only to the lowest empty energy level.The irregular structure of the QD can also complicate the description of electron transport. Therefore, describing transport through the QD by transmission amplitudes is better adapted to the problem.

A quantum mechanic tool to describe such a system is the scattering matrix $\hat{S}$. It relates the scattering states of incoming and outgoing electrons, which are scattered by a quantum dot, cf. Figure 1.5:

$$\vec{\psi}^{out} = \hat{S}\vec{\psi}^{in} \tag{1.2}$$

It is important to notice, that in this case, the scattering matrix does not only depend on the properties of the dot but also on the coupling of the dot to the leads. This coupling usually consists of a contraction of the lead at the lead-dot interface,

see Figure 1.1. Such a contraction is called a quantum point contact (QPC) under some conditions, which will be described later.

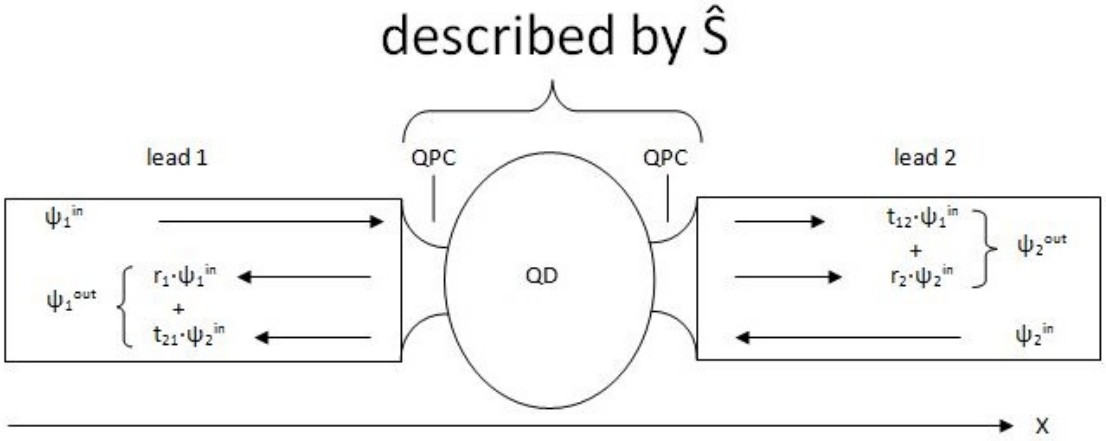

Figure 1.5.: Two leads connected to a quantum dot, which represents the scattering area. Each lead has one transmitting channel with incoming and outgoing states.

Here $\psi_{1,2}^{in}$ and $\psi_{1,2}^{out}$ in lead 1 and 2 are the wavefunctions for incoming and outgoing electrons. Before going into more details about the scattering matrix, the nature of the leads should be specified . As stated earlier, the leads are confined by the electric field of the gate wires placed on top of the conduction material. These fields should be strong enough, so that the resulting potential for the electrons can be described by an infinite potential well in every direction perpendicular to the lead (y-,z-direction) and by a potential constant in x-direction (parallel to the wire). For simplicity, we consider non-interacting leads, so electron-electron interactions will be neglected and the electrons inside the leads form a free electron gas. This assumption is valid for experiment if the applied voltage is small enough so electrons move one by one through the leads. Electrons can only travel in one dimension (the x-direction), therefore the leads can be described as ideal waveguides with a wavefunction factorized into a part in x-direction and a part in y- and z-direction. The latter is the solution of the infinite potential well and therefore consists of standing waves with quantized energy levels E_n, which are also called channels. Only the channels with $E_n < E_F$, where E_F is the Fermi energy, can be occupied by electrons and therefore contribute to electron transport. These channels are called "open" and their number is finite. Since the energy levels of an infinite potential well E_n are proportional to L^{-2}, with L the transverse size of the wire, the number of open channels can be reduce by making the leads narrower. A contraction of the width of the wire $L(x)$ is called a QPC if the factorization of the total wavefunction is still possible. This is true if the change of width is adiabatic, which means following equations are true:

$$\left|\frac{dL(x)}{dx}\right| \ll 1 \quad \text{and} \quad L(x)\left|\frac{d^2L(x)}{dx^2}\right| \ll 1$$

A QPC enables to tune the number of open channels. Since the potential is constant the wavefunction in x-direction is plane waves far from the QPC. For simplicity, we consider only one channel in every lead. The incoming waves can either be reflected from the dot or transmitted through the dot. So the outgoing waves consist of a reflected and a transmitted part. In Figure 1.5 the reflection amplitudes r_1 and r_2 are introduced, which describe the reflection from the dot back into lead 1 and 2 respectively. Equivalently, the transmission amplidutes t_{12} and t_{21} describe transmission from one lead to the other, from 1 to 2 and from 2 to 1 respectively. All these amplitudes can be complex. The outgoing states read:

$$\psi_1^{out} = r_1\psi_1^{in} + t_{21}\psi_2^{in} \ , \quad \psi_2^{out} = t_{12}\psi_1^{in} + r_2\psi_2^{in} \ .$$

With $\vec{\psi}^{out} = (\psi_1^{out}, \psi_2^{out})^T$ and $\vec{\psi}^{in} = (\psi_1^{in}, \psi_2^{in})^T$ one can define the scattering matrix from (1.2):

$$\hat{S} = \begin{pmatrix} r_1 & t_{12} \\ t_{21} & r_2 \end{pmatrix} \tag{1.3}$$

The $\hat{S}$ matrix is unitary($\hat{S}^\dagger = \hat{S}^{-1}$) due to particle conservation [5]. As a result, $|t_{12}| = |t_{21}| = T$ and $|r_1| = |r_2| = R$ with $R^2 + T^2 = 1$. If the scattering process is time reversal, the S-matrix is also symmetric ($\hat{S}^T = \hat{S}$), so $\vec{\psi}^{in}$ and $\vec{\psi}^{out}$ can be exchanged in (1.2). In a more general case, there are N_{ch} channels in every lead and reflection and transmission processes can occour between any channels. This will not affect the general structure or properties of the scattering matrix, but only change r_1, r_2 and t_{12}, t_{21} to $N_{ch} \times N_{ch}$ matrices, where, for example, an entry $\left(\hat{t}_{21}\right)_{kl}$ describes the transmission amplitude for a plane wave coming from channel l in the second lead and going to the channel k in the first lead. The unitarity of the scattering matrix generaly leads to $\hat{t}_{12}\hat{t}_{12}^\dagger$, $\hat{t}_{12}^\dagger\hat{t}_{12}$, $\hat{t}_{21}\hat{t}_{21}^\dagger$ and $\hat{t}_{21}^\dagger\hat{t}_{21}$ having the same eigenvalues $\{T_P\}$. Furthermore the eigenvalues $\{R_P\}$ of $\hat{r}_1\hat{r}_1^\dagger$, $\hat{r}_1^\dagger\hat{r}_1$, $\hat{r}_2\hat{r}_2^\dagger$ and $\hat{r}_2^\dagger\hat{r}_2$ are the same with $\{T_P\} + \{R_P\} = 1$.
The current through the system can be described with the help of the Landauer formula, which uses the scattering matrix. By performing time and quantum mechanic averaging, one can derive a formula for the current measured in experiment:

$$\langle\langle\hat{I}\rangle_t\rangle_{QM} = \frac{G_Q}{e}\int_0^\infty dE \sum_p T_p(E)\left[f_1(E) - f_2(E)\right]$$

Here $f_i(E)$ is the Fermi distribution function and $T_P(E)$ describe the energy dependence of the eigenvalues.

Since the electron wavefunctions are plane waves in the leads, it is interesting to look at interference experiments of these electrons. One setup for this kind of experiment provides the so called Aharonov-Bohm (AB) ring, which will be described

following [9]. The basic structure is demonstrated in Figure 1.6. Two wires in the middle form a ring-like structure, which is connected to the outside via another two leads. The connecting junctions can be described by 3×3 scattering matrices, since every electron can either be reflected into the lead it comes from or transmitted into one of the two wires. If a bias voltage is applied to the left (electron source) and right lead (electron drain), electrons move through the ring. This bias should be small enough, so that the bias drops completly at the two junctions and electrons can move freely inside the ring. This way electrons can be reflected at the two junctions multiple times before leaving the ring. The electrons aquire a phase depending on the path covered from source to drain and any applied scalar or vector potential to the ring. The electron waves interfere in the drain lead, which results in the transmission amplitude for the whole system. The aquired phase of the electrons has two contributions, namely the dynamical phase χ_t and the magnetic phase ϕ_t. χ_t depends on the total distance an electron covers inside the ring but not the direction in which the path is run through. It is therefore sample dependent. Furthermore, the dynamical phase depends on the electron energy and any scalar potential in the ring. Denoting the phase aquired in the upper arc of the ring by χ_1 and in the lower arc by χ_2, the dynamical phase reads: $\chi_t = n_1\chi_1 + n_2\chi_2$, with n_i the number of passes through the i-th wire.

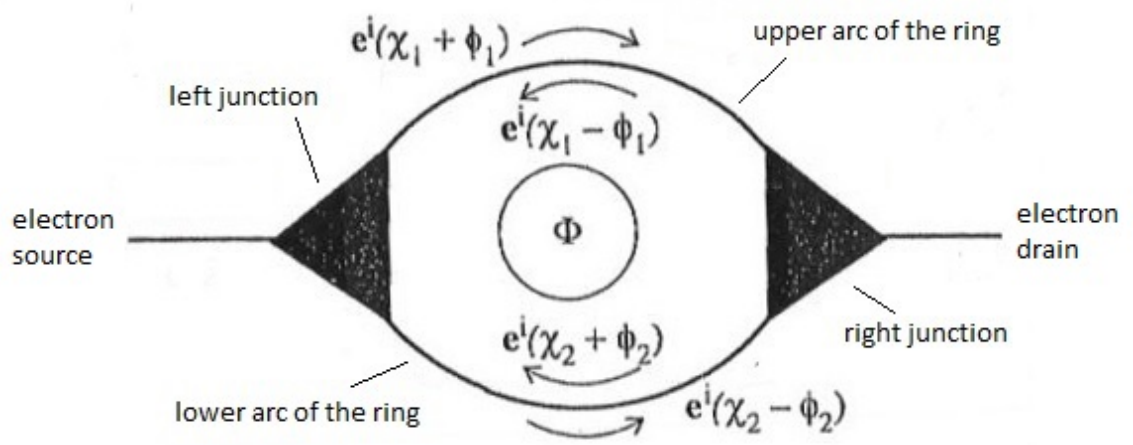

Figure 1.6.: The structure of an AB ring connected to an electron source and drain. The Φ in the middle of the ring denotes a magnetic flux arising from an applied magnetic vector potential. The picture was taken from [9]

ϕ_t does depend on the direction in which a path is run through. This results in different signs for the phase of counter clockwise and clockwise propagating electrons in the ring. the absolute value of ϕ_t depends on the magnetic flux through the ring thus, it depends on the vector potential of the magnetic field and not the magnetic field itself. The gauge degree of freedom of the magnetic vector potential translates to $\phi_t(\vec{A})$, which is therefore also not gauge invariant. Since the total transmission of the system must be gauge invariant, one has to find a gauge invariant quantity

depending on the magnetic phase. This quantity is the phase aquired by a closed loop with winding number one and can be calculated as $\phi_l = \frac{\pi\Phi}{\Phi_0}$, with Φ the magnetic flux through the ring and $\Phi_0 = \frac{hc}{2e}$ the flux quantum. Since ϕ_t only depends on the loop number n_l and the flux through the ring, it is sample independent. Denoting the magnetic phase in the upper arc of the ring by ϕ_1 and in the lower arc by ϕ_2, one can find:

$$\phi_t = n_l\phi_l + \begin{cases} -\phi_1, & \text{if the particle passes lead 1 first} \\ +\phi_2, & \text{if the particle passes lead 2 first} \end{cases}$$

Here n_l is the number of clockwise loops minus the number of counter-clockwise loops and we define: $\phi_l = \phi_1 + \phi_2$. The total phase θ_k aquired for a certain path labeled by k is the sum of $\chi_{t,k}$ and $\phi_{t,k}$. For real valued scattering matrices the transmission through the ring reads:

$$T = \left|\sum_k A_k e^{i\theta_k}\right|^2 = \sum_{k,n} A_k A_n e^{i(\theta_k-\theta_n)} = \sum_{k,n} A_k A_n e^{i(\chi_{t,k}-\chi_{t,n}+\phi_{t,k}-\phi_{t,n})} =$$

$$= T_{cl} + T_{qm}$$

$$\text{with} \quad T_{cl} = \sum_k A_k^2 \quad \text{and} \quad T_{qm} = \sum_{k\neq n} A_k A_n \cos\left(\chi_{t,k} - \chi_{t,n} + \phi_{t,k} - \phi_{t,n}\right) \ . \quad (1.4)$$

T_{cl} and T_{qm} are the classical and quantum contribution to the transmission, respectively. A_k are weights taking into account the probability of a path k and can be calculated from the two scattering matrices representing the left and right junction. T_{qm} is gauge invariant, since the gauge dependent parts ϕ_1 and ϕ_2 of $\phi_{t,k} - \phi_{t,n}$ either cancel each other or add up to a full loop in clockwise or anti-clockwise direction. T_{qm} can be further split into two contributions, a part dependent and a part independent of the dynamical phases $\chi_{t,k}$. The former part with $\chi_{t,k} \neq \chi_{t,n}$ vanishes when taking the ensemble average over $\chi_{t,k}$. In experiment this can be realised by performing conductance measurements for either different ring setups, thus changing the length of the two arcs forming the ring, or for different chemical potentials in the ring leads, and therefore using the energy dependence of the dynamical phase to change it. The second part of T_{qm} with $\chi_{t,k} = \chi_{t,n}$ will not vanish in an ensemble average, since the magnetic phase is independent of the sample. The arguments of the cosine functions contributing to this part have the structure $\phi_{t,k} - \phi_{t,n} = 2m\phi_l = 2m\frac{\pi\Phi}{\Phi_0}$, with integer m. Therefore, contributions to T_{qm}, which do not depend on the dynamical phases, are periodically maximal at the same flux $\Phi = s\Phi_0$, with s a number. Any perodical dependency of a physical quantitiy on $\frac{\Phi}{\Phi_0}$, like the transmission amplitude in an AB ring, is called the Aharonov-Bohm effect.

In state of the art expermients, AB rings and QDs are combined. For example, the QD can be put into one arm of the AB ring, see the last panel of Figure 1.1. It was shown in [4], that coherent electron transport through a quantum dot is possible if

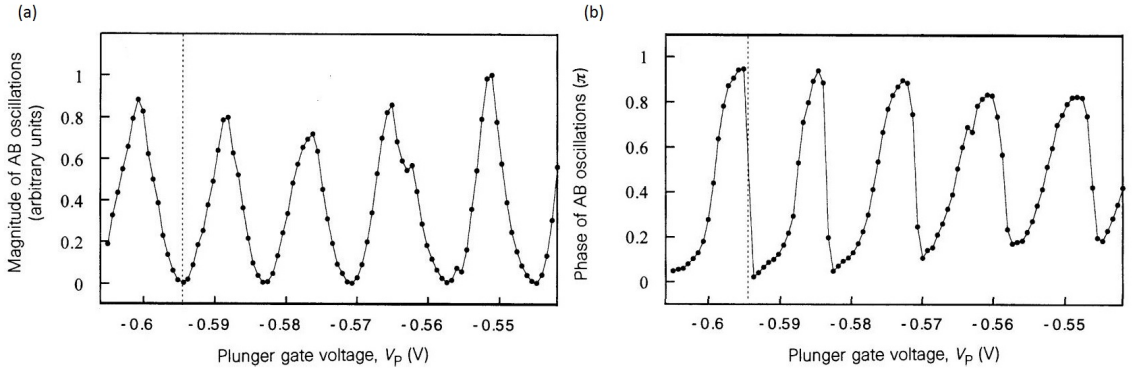

Figure 1.7.: The experimental results of the transmission of a QD in an AB ring published in [6]. (a) The CB peaks and valleys of a sole quantum dot are clearly visible. The peak values vary between 0.8 and 1.0 while the valleys always go down to zero. (b) The phase continously increases from zero to π in the range of one CB peak and abruptly jumps down by π everytime the transmission amplitude goes to zero.

the coupling of the QD to the leads is strong enough. In this case, the AB effect still affects the total transmission amplitude of the system. By changing the flux and recording the resulting oscillations of the current through the system in the linear response regime, information about the quantum dot, for example the transmission amplitude, can be calculated. This is done by adding more junctions to the ring leads, at which electrons can leave the ring. This reduces the probability for an electron to pass a whole arc of the ring and paths covering more than one lead are neglectable in the sums of (1.4). A more detailed theory is presented in [10]. The transmission amplitude of the dot in the AB ring can be written as $T_d = |T_d|e^{i\alpha}$, transmission through the dot occurs with an amplitude $|T_d|$, but transmission also adds a phase α to the electron wave. Both quantities depend on the gate voltage applied to the QD. Figure 1.7 shows experimental data from [6], where a setup containing a "large" quantum dot with about 200 electrons was used. $|T_d(V_g)|$ shows the typical coulomb blockade peaks and valleys, which are almost periodic, see Figure 1.7 (a). Between two CB peaks $\alpha(V_g)$ increases continously by π, as expected for such a system, but when the transmission amplitdue goes to zero in the CB valley the phase abruptly jumps by π. This effect is called a phase lapse and its occurrence is found to be universal in this data, which means there is a phase laps in every CB valley. Therefore, it cannot be explained by microscopic details of the dot, which are in general not known. For example, the unknown shape of the dot governs random energy levels. If phase lapses were sensitive to such details, their appearance would also seem to be random. In another experiment [7], which used a smaller QD with a maximum of 20 electrons, a so called mesoscopic regime was discovered. This is a regime, in which the observed physics is sensitive to microscopic details, but since they are not known, the behaviour seems to be random. The mesoscopic regime

emerges if 10 or less electrons are in the dot [7]. The more electrons are in a QD the smaller is its levelspacing and the higher becomes the charging energy of the dot. To investigate whether these quantities trigger the change from the mesoscopic to the universal regime, a numerical approach, focusing on the interplay between the level spacing δ_j of the energy levels of the dot, their widths Γ_j and the charging energy U, was done in [8].
The model used in this numerical simulation consists of three parts. Firstly spinless electrons in the QD are described by the Hamiltonian:

$$\hat{H}_{dot} = \sum_{j=1}^{N} \varepsilon_j \hat{n}_j + \frac{1}{2} U \sum_{j \neq j'} \left(\hat{n}_j - \frac{1}{2} \right) \left(\hat{n}_{j'} - \frac{1}{2} \right) \tag{1.5}$$

whwew N is the number of levels contributing to the transmission, ε_j is the energy and $\hat{n}_j = \hat{d}_j^\dagger \hat{d}_j$ the particle number operator of the j-th state. $\hat{d}_j^\dagger / \hat{d}_j$ are the creation/annihilation operators for spinless electrons of the j-th state in the dot. $U > 0$ describes the Coulomb interaction inside the dot and is therefore a charging energy which seperates the CB peaks. The energy levels of the dot can be shifted by the gate voltage and define the single particle level spacing $\delta_j = \varepsilon_{j+1} - \varepsilon_j$ and the mean level spacing $\Delta = \frac{1}{N} \sum_j \delta_j$.
The second part of the model is the Hamiltonian for the leads:

$$\hat{H}_l = -t \sum_{m=0}^{\infty} \left(\hat{c}_{m,l}^\dagger \hat{c}_{m+1,l} + h.c. \right) \tag{1.6}$$

which describes a semi-infinite tight-binding chain with a zero on-site energy. t is the hopping amplitdue and $\hat{c}_{m,l}^\dagger / \hat{c}_{m,l}$ the creation/annihilation operators for the m-th site of the lead l. Two leads, left and right, were used in this paper, so $l = L, R$. The site with $m = 0$ is the one closest to the QD, see Figure 1.8. The Hamiltonian describes a system, in which only one electron per site is allowed, so electrons move one by one. Furthermore the electrons can only hop to their nearest neighbours.
The last part of the model describes the lead-dot coupling:

$$\hat{H}_T = -\sum_{j,l} \left(t_j^l \hat{c}_{0,l}^\dagger \hat{d}_j + h.c \right) \quad . \tag{1.7}$$

Here t_j^l are the coupling amplitudes for the j-th channel inside the dot and the l-th lead connected to the dot. The site $m = 0$ of the lead is coupled to the QD, see Figure 1.8. The coupling amplitudes define the level width via $\Gamma_j = \sum_l \pi \nu |t_j^l|^2$ where ν is the local energy-independent density of states of the lead, calculated on the site $m = 0$.
By assuming a constant level spacing δ, it was observed, that if $\delta \leq \Gamma$ and $|\Gamma - \delta| \ll \delta$, as many energy levels as leads attached to the QD become much wider than the others. Furthermore the position of these broad levels as a function of gate voltage is almost constant over a large interval of V_g if $U \neq 0$. In this interval, the energy of the broad levels is close to the chemical potential of the leads. After changing the

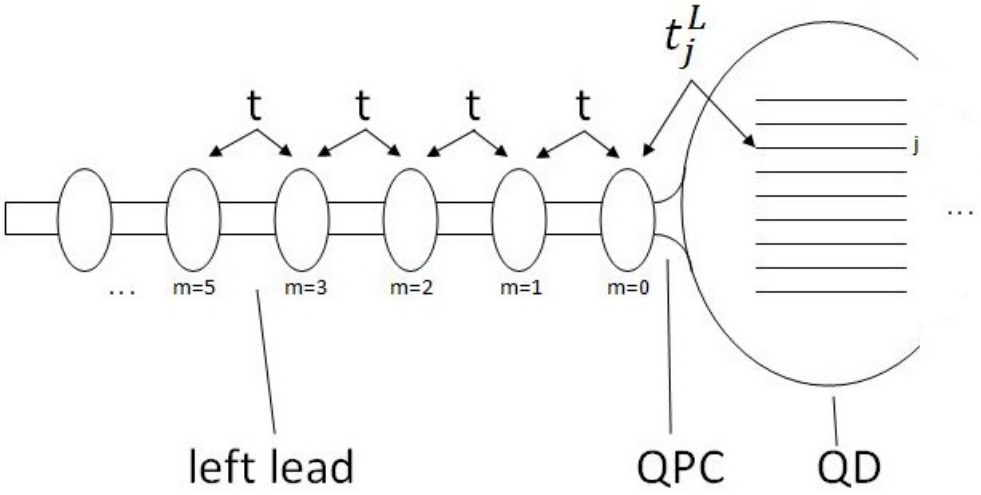

Figure 1.8.: Sketch of the tight binding model for the left lead.

gate voltage in this interval, the remaining narrow energy levels cross the wide ones. This overlap enables electron transport in two or more energy levels simultaniously, which leads to interference effects. The transmission zero accopanying every phase lapse indicates destructive interference between transmitting channels. Interferences in a setup of a discrete energy level overlapping with a continuum of possible energies, can be described by Fano-type antiresonances, which are accompanied by a phase lapse [13]. The discrete energy level can be identified with a narrow energy level and the continuum with a broad energy level [8]. To summarize, the important conditions for the occurence of a phase lapse are $\delta \leq \Gamma$, $|\Gamma - \delta| \ll \delta$ and $U \neq 0$. It was noticed that the the broad energy levels exist for $U = 0$ aswell. Some of the results of numericial calulations in the universal regime can be seen in Figure 1.9. The red line is the position of the broad energy level. It is almost constant for a wide range of gate voltage. Everytime one of the three narrow energy levels crosses the red line a phase laps and transmission zero occurs. For $U \geq \Gamma$ the CB peaks are well seperated and the typical behaviour of phase can be observed. By further increasing the charging energy to $U \gg \Gamma$, the resulting curve matches the experimental results.

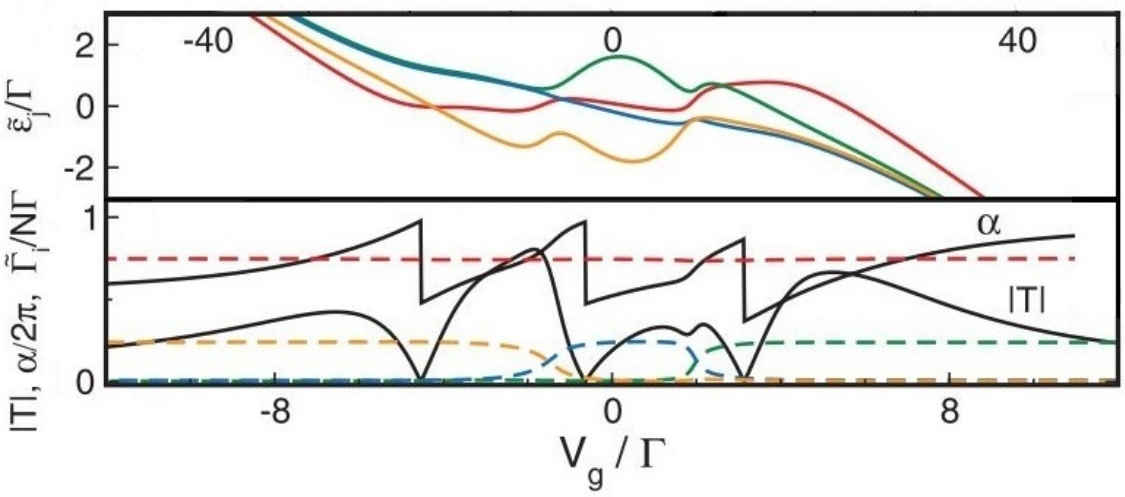

Figure 1.9.: The top panel shows the energy levels of the dot changing with gate voltage. The Fermi level of the lead was set to zero. The red line is the position of the broad energy level which is almost zero for a wide range of V_g. The phase and the absolute vlaue of the transmission amplitude are plotted in the lower panel. The data was taken from [8].

2. The emergence of the broad energy levels

The presented explanation for the phase lapses taken from [8] depends crucially on the existence of the broad energy levels. The Hamiltonian for the dot and a constant level spacing was assumed for the simulations. It was proposed, that a small deviation from the latter assumption does not change the results. However the assumption about a regular nature of the QD spectrum and even more importantly, about the specific lead-dot coupling considered in [8] can substantially disagree with experiments. In particular, the energy levels inside the dot are not known and very random. Also the coupling of the QD to the leads can be very different. For example a lead can be connected to many levels inside the dot or only to a few. But since the phase lapses occur in different QDs, the explanation of this effect must not depend the assumption of constant level spacing or a specific coupling. Therefore it is left to study, whether the occurence of the broad energy levels depends on the above mentioned assumptions or if it is a more general effect arising from the generic coupling to the leads. A more general model, which can be derived from microscopic assumptions and takes the randomness of the QD into account will be studied in this thesis. The focus will be on the occurance and stability of the broad energy levels and on finding the relevant regimes where it appears. This is done by numerically diagonalizing the Hamiltonian of the system. The distribution of the energy widths will be investigated and its dependencies on the number of levels inside the dot and the strength of the coupling between the dot and the lead will be studied. Furthermore a generalization of the description for the QPC will be suggested.

3. The random matrix approach

3.1. The total Hamiltonian

The model, that is used in this thesis, consists of three parts which describe spinless, non-interacting electrons. Furthermore, we put $\hbar = 1$ for the whole thesis. The first part is $\hat{H}_D$, describing the QD, the second is $\hat{H}_L$, describing the leads and the last is $\hat{H}_{LD}$, describing the coupling of the leads to the QD and therefore resembles the QPC. Since properties of electron transport, which mostly origins from electrons with energies close to the Fermi energy, are of interest, the electrons in the leads can be discribed by the linearized, one dimensional dispersion relation of a free electron gas. By assuming non-interacting leads, $\hat{H}_L$ reads:

$$\hat{H}_L = v_F \sum_{j=1}^{N_{ch}} \int \frac{dk}{2\pi} k \hat{\psi}_j^\dagger(k) \hat{\psi}_j(k) \quad . \tag{3.1}$$

Here N_{ch} is the number of open channels in the lead, v_F is the Fermi velocity and k is the wavevector relative to the Fermi level; $\hat{\psi}_j^\dagger(k)/\hat{\psi}_j(k)$ are the fermionic creation/annihilation operators for electrons in channel j in momentum representation. If more than one lead is attached to the QD, N_{ch} is the sum of the open channels in every lead. Assuming a random potential U inside the QD, $\hat{H}_D$ reads:

$$\hat{H}_D = \int d\vec{r} \left[\frac{1}{2m} \vec{\nabla} \hat{a}^\dagger \vec{\nabla} \hat{a} + U \hat{a}^\dagger \hat{a} \right]$$

with electron creation/annihilation operators $\hat{a}^\dagger/\hat{a}$ and electron mass m. It is known [2] that such a Hamiltonian can be split into two parts: a universal part $\hat{H}^{(0)}$, which is corresonds to $g \to \infty$, and a non-universal part $\hat{H}^{(1/g)}$, which is proportional to g^{-1}. Since $g >> 1$, $\hat{H}^{(1/g)}$ is small and will be neglected. Since interactions [11] are neglected in this thesis, the Hamiltonian for the QD reads:

$$\hat{H}_D = \sum_{\alpha,\gamma=1}^{M} H_{\alpha\gamma} \hat{\phi}_\alpha^\dagger \hat{\phi}_\gamma \quad . \tag{3.2}$$

M is the number of energy levels in the QD and $\hat{\phi}_\alpha^\dagger/\hat{\phi}_\alpha$ are the respective creation annihilation operators. $H_{\alpha\gamma}$ are the entries of a random hermitian $M \times M$ matrix ($H = H^\dagger$) from the WD Gaussian ensemble. Its elements are Gaussian distributed with the correlation function

$$\langle H_{\alpha\gamma} H_{\alpha'\gamma'} \rangle = \frac{M\Delta^2}{\pi^2} \left[\delta_{\alpha\gamma'}\delta_{\alpha'\gamma} + \left(\frac{2}{\beta} - 1 \right) \delta_{\alpha\alpha'}\delta_{\gamma\gamma'} \right] \quad . \tag{3.3}$$

Here β is the Dyson symmetry parameter, which reflects time-reversal symmetry. For $\beta = 1$ the system has time-reversal symmetry resulting in H real and for $\beta = 2$ the system has no time-reversal symmetry resulting in H complex with equal variances of imaginary and real parts of H_{ij}. For simplicity, time-reversal symmetry is assumed ($\beta = 1$) in this thesis. $\Delta = \pi M^{-1/2}$ is the mean, one electron level spacing for a Gaussian orthogonal distribution in the dot [14], so (3.3) reduces to:

$$\langle H_{\alpha\gamma} H_{\alpha'\gamma'} \rangle = \delta_{\alpha\gamma'}\delta_{\alpha'\gamma} + \delta_{\alpha\alpha'}\delta_{\gamma\gamma'} \quad . \tag{3.4}$$

The last part of the model is the coupling of the lead to the dot:

$$\hat{H}_{LD} = \sum_{j=1}^{N_{ch}} \sum_{\alpha=1}^{M} \int \frac{dk}{2\pi} \left[W_{\alpha j} \hat{\phi}_\alpha^\dagger \hat{\psi}_j(k) + W_{\alpha j} \hat{\psi}_j^\dagger(k) \hat{\phi}_\alpha \right] \quad . \tag{3.5}$$

Here $W_{\alpha j}$ are the elements of a real $M \times N_{ch}$ matrix ($W = W^*$) describing the coupling of the dot and the lead, so this parameter represents the QPC. The total Hamiltonian is the sum of the three parts:

$$\hat{H}_{tot} = \hat{H}_D + \hat{H}_L + \hat{H}_{LD} \quad . \tag{3.6}$$

3.2. Impact of the leads on the dot

Since we focus on the properties of the QD, the leads will be integrated out in $\hat{H}_{tot}$ to find an effective Hamiltonian $\hat{H}_{eff}$ describing only the QD and the QPC. We can write the total Hamiltonian as:

$$\hat{H}_{tot} = \hat{H}_L \otimes \mathbb{1}_D + \mathbb{1}_L \otimes \hat{H}_D + \hat{H}_{LD} \quad .$$

The wavefunction it acts on has the structure: $|\psi_L\rangle \otimes |\psi_D\rangle$, with a wavefunction for the lead $|\psi_L\rangle$ and the dot $|\psi_D\rangle$. To find $\hat{H}_{eff}$, a quantum mechanic averaging with the groundstate wavefunction of the lead is performed: $\hat{H}_{eff} = \langle \hat{H}_{tot} \rangle_L$. $\langle \hat{H}_L \rangle_L \mathbb{1}_D$ is a number and can therefore be neglected. $\langle \mathbb{1}_L \rangle_L \hat{H}_D = \hat{H}_D$ since the wavefunctions are normalized. The expectation value of the Hamiltonian for the coupling of the lead and the dot $\langle \hat{H}_{LD} \rangle_L$ yields the self energy Σ in a Green's function approach. The Dyson's equation for a Green's function for the dot reads:

$$\hat{G}_D^{-1}(\varepsilon = 0) = \left(\hat{G}_D^0(\varepsilon = 0) \right)^{-1} - \hat{\Sigma} \tag{3.7}$$

Where $\hat{G}_D^0(\varepsilon = 0) = \left(\hat{H}_D \right)^{-1}$ and $\hat{G}_D(\varepsilon = 0) = \left(\hat{H}_{eff} \right)^{-1}$. $\hat{\Sigma}$ describes a hopping of electrons to and from the QD. The only non vanishing contribution to $\hat{\Sigma}$ is

$\langle \hat{H}_{LD}\hat{H}_{LD}\rangle_L$. It describes an electron hopping to the lead and back to the dot again without any propagation in the lead, so it depends on the Green's function in the lead at $x = 0$: $\hat{G}^0_L(0,0;\omega)$. For easier calculations, the basis of $\hat{\psi}^\dagger_j(k)/\hat{\psi}_j(k)$ in $\hat{H}_{LD}$ will be changed from momentum to real space represantation.

$$\hat{\psi}_j(k) = \int dx \langle k|x\rangle \hat{\psi}_j(x) = \int dx\ e^{-ikx}\hat{\psi}_j(x) \tag{3.8}$$

$$\hat{\psi}^\dagger_j(k) = \int dx \langle x|k\rangle \hat{\psi}^\dagger_j(x) = \int dx\ e^{ikx}\hat{\psi}^\dagger_j(x) \tag{3.9}$$

This yields $\hat{H}_{LD}$ in real space representation:

$$\hat{H}_{LD} = \sum_{j=1}^{N_{ch}} \sum_{\alpha=1}^{M} \left[W_{\alpha j}\hat{\phi}^\dagger_\alpha \hat{\psi}_j(0) + W_{\alpha j}\hat{\psi}^\dagger_j(0)\hat{\phi}_\alpha \right] \quad . \tag{3.10}$$

By using

$$\langle \hat{\psi}^\dagger_i(x)\hat{\psi}^\dagger_{,j}(x)\rangle_L = \langle \hat{\psi}_i(x)\hat{\psi}_j(x)\rangle_L = 0\ \forall i,j$$

$$\langle \hat{\psi}^\dagger_i(x)\hat{\psi}_j(x)\rangle_L = \langle \hat{\psi}_i(x)\hat{\psi}^\dagger_j(x)\rangle_L = 0 \text{ for } i \neq j$$

we find with omitting $x = 0$ dependencies:

$$\begin{aligned}
\langle \hat{H}_{LD}\hat{H}_{LD}\rangle_L &= \sum_{\alpha,\beta=1}^{M} \sum_{j=1}^{N_{ch}} W_{\alpha,j}W_{\beta,j} \left[\langle \hat{\psi}_j\hat{\psi}^\dagger_j\rangle_L \hat{\phi}^\dagger_\alpha\hat{\phi}_\beta + \langle \hat{\psi}^\dagger_j\hat{\psi}_j\rangle_L \hat{\phi}_\alpha\hat{\phi}^\dagger_\beta \right] = \\
&= \sum_{\alpha,\beta=1}^{M} \sum_{j=1}^{N_{ch}} W_{\alpha,j}W_{\beta,j} \left[\langle \hat{\psi}_j\hat{\psi}^\dagger_j\rangle_L \hat{\phi}^\dagger_\alpha\hat{\phi}_\beta + \langle \hat{\psi}^\dagger_j\hat{\psi}_j\rangle_L \hat{\phi}_\beta\hat{\phi}^\dagger_\alpha \right] = \\
&= \sum_{\alpha,\beta=1}^{M} \hat{\phi}^\dagger_\alpha \underbrace{\left[\langle \hat{\psi}_j\hat{\psi}^\dagger_j\rangle_L - \langle \hat{\psi}^\dagger_j\hat{\psi}_j\rangle_L \right]}_{=i\hat{G}^0_L} \left[WW^\dagger\right]_{\alpha\beta} \hat{\phi}_\beta = \\
&= \sum_{\alpha,\beta=1}^{M} \hat{\phi}^\dagger_\alpha \left(i\hat{G}^0_L \left[WW^\dagger\right]_{\alpha\beta} \right) \hat{\phi}_\beta \quad .
\end{aligned} \tag{3.11}$$

By using the Feynman rules [15], one can express the self energy as: $\Sigma_{\alpha\beta} = -iV_{\alpha\beta}\hat{G}^0_L$. It follows from (3.11) that $V_{\alpha\beta} = i\left[WW^\dagger\right]_{\alpha\beta}$. $\hat{G}^0_L(0,0;\omega) = \mp\pi i\nu(\omega)$ [5], $\nu(\omega) \approx \nu(\varepsilon_F) = \nu$ is the density of states in the lead at the Fermi energy, since $\omega \approx \varepsilon_F$. The sign of $\hat{G}^0_L$ must correspond to the retardation ($-$ retarded, $+$ advanced). In total the selfenergy reads:

$$\Sigma_{\alpha\beta} = \mp i\pi\nu \left[WW^\dagger\right]_{\alpha\beta} \quad . \tag{3.12}$$

The effective Hamiltonian with the retarded self energy reads:

$$\hat{H}_{eff} = \sum_{\alpha,\beta=1}^{M} \left(H_{\alpha\beta} + i\pi\nu \left[WW^{\dagger} \right]_{\alpha\beta} \right) \hat{\phi}_{\alpha}^{\dagger} \hat{\phi}_{\beta} \quad . \tag{3.13}$$

The coupling of the leads to the dot yields an imaginary contribution to the eigenvalues. The imaginary part of the eigenvalues of (3.13) determines the life timeof the state, which is inverse to the level broadening. The highest possible rank of the matrix $WW^{\dagger}$ is the number of channels in the leads N_{ch} by construction. So the number of non zero eigenvalues of the selfenergy matrix is N_{ch} and the number broadened energy levels is expected to be also N_{ch} [8].

4. Description of the QPC

To find the coupling matrix W, the scattering matrix for the whole system will be derived and seperated in parts originating from the QD and the QPC.

4.1. Deriving the S-matrix for the whole system

This section follows the Appendix C of [2]. As stated in the introduction, the S-matrix relates incoming and outgoing electrons. Equation (1.2) for each channel takes the form:

$$a_i^{out} = \sum_{j=1}^{N_{ch}} S_{ij} a_j^{in} \tag{4.1}$$

with a_i^{out}/a_j^{in} the amplitudes of the outgoing/incoming electrons in channel i/j. We assume that the 1-D interference is at $x = 0$, see Figure [**?**].

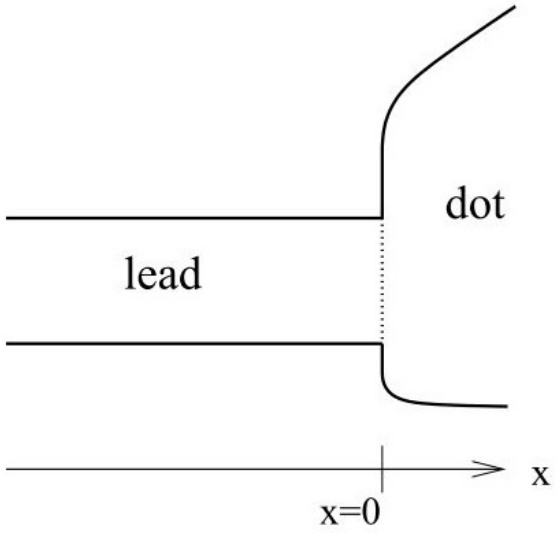

Figure 4.1.: Definition of the coordinates at a lead-dot interface. The picture was taken from [2].

As explained in the introduction, the wavefunction for all electrons in the lead consists of plane wave contributions with an amplitude $\Phi_j(\vec{r}_\perp)$ depending on the perpendicular coordinates. With $k = \frac{\varepsilon}{v_F}$, the wavefunction reads:

$$\psi_e(\vec{r}) = \sum_{j=1}^{N_{ch}} \Phi_j(\vec{r}_\perp) \left[a_j^{in} e^{i\left(k_F + \frac{\varepsilon}{v_F}\right)x} + a_j^{out} e^{-i\left(k_F + \frac{\varepsilon}{v_F}\right)x} \right] \tag{4.2}$$

The corresponding annihilation operator can be written as:

$$\hat{\psi}_e(\vec{r}) = \sum_{j,l=1}^{N_{ch}} \Phi_j(\vec{r}_\perp) \int \frac{dk}{2\pi} \left[U_{jl}^* e^{i(k_F+k)x} + U_{jl} e^{-i(k_F+k)x} \right] \hat{\psi}_j(k) \tag{4.3}$$

where U describes the boundary conditions at $x = 0$. If there is no coupling to the dot, electrons will be reflected at $x = 0$, resulting in a phaseshift of π without mixing channels. This way all channels are incorporated into one matrix. The Dirichlet boundary condition, $\hat{\psi}_e(0) = 0$ yields $U_{jl} = i\delta_{jl}$, if the boundary is an infinite wall. For easier calculations, the basis of $\hat{\psi}_j^\dagger(k)/\hat{\psi}_j(k)$ in $\hat{H}_L$ will be changed from momentum to real space represantation, see equations (3.8) and (3.9). The result reads:

$$\hat{H}_L = -iv_F \sum_{j=1}^{N_{ch}} \int dx \; \hat{\psi}_j^\dagger(x) \frac{d}{dx} \hat{\psi}_j(x) \quad . \tag{4.4}$$

Denoting the single electron wavefunctions for each channel in the lead by ψ_j and in the dot by ϕ_α and the ground state by ψ_0 in the leads and ϕ_0 in the dot respectivly, the creation/annihilation operators act as follows:

$$\hat{\psi}_j(x')\psi_i(x) = \delta_{ij}\delta(x - x')\psi_0 \tag{4.5}$$

$$\hat{\psi}_j^\dagger(x)\psi_0 = \psi_j(x) \tag{4.6}$$

$$\hat{\phi}_\alpha \phi_\gamma = \delta_{\alpha\gamma}\phi_0 \tag{4.7}$$

$$\hat{\phi}_\alpha^\dagger \phi_0 = \phi_\alpha \tag{4.8}$$

Writing down the Schrödinger equation with the total Hamiltonian (3.6) for the leads, with the wavefuntion $\psi_i(x) \otimes \phi_0$, and for the dot, with the wavefuntion $\psi_0 \otimes \phi_\alpha$, yields the equations:

$$\varepsilon\psi_i(x) = iv_F \frac{d\psi_i(x)}{dx} + \sum_{\alpha=1}^{M} W_{\alpha i}^* \delta(x)\phi_\alpha \tag{4.9}$$

$$\varepsilon\phi_\beta = \sum_{\alpha=1}^{M} H_{\beta\alpha}\phi_\alpha + \sum_{j=1}^{N_{ch}} W_{\beta j}\psi_j(0) \tag{4.10}$$

At $x < 0$, equation (4.9) describes a left moving particle. Using (4.2), (4.9) and (4.10), we can find $\psi_j(x)$:

$$\psi_j(x) = \begin{cases} e^{-ikx} \sum_{l=1}^{N_{ch}} U_{jl} a_l^{in}, & x = +0 \\ \frac{1}{2} \sum_{l=1}^{N_{ch}} \left(U_{jl} a_l^{in} + U_{jl}^* a_l^{out} \right), & x = 0 \\ e^{-ikx} \sum_{l=1}^{N_{ch}} U_{jl}^* a_l^{out}, & x < 0 \end{cases} \tag{4.11}$$

with the proper normalization at $x = 0$. The unknown wavefunction inside the QD can now be eliminated with (4.9) and (4.10). But before the divergence in (4.9) at $x = 0$ has to be taken care of. Let us integrate over x from $-\epsilon$ to ϵ in the limit $\epsilon \to 0$:

$$\varepsilon \underbrace{\lim_{\epsilon \to 0} \int_{-\epsilon}^{\epsilon} \psi_j(x) dx}_{\to 0, \text{ since } \psi_j(0) \text{ finite}} = \lim_{\epsilon \to 0} \int_{-\epsilon}^{\epsilon} i v_F \frac{\partial \psi_j(x)}{\partial x} dx + \lim_{\epsilon \to 0} \int_{-\epsilon}^{\epsilon} \sum_{\nu=1}^{M} W_{\nu j}^* \delta(x) \phi_\nu dx$$

$$\Rightarrow 0 = \lim_{\epsilon \to 0} i v_F \left(\psi_j(+\epsilon) - \psi_j(-\epsilon) \right) + \sum_{\nu=1}^{M} W_{\nu j}^* \phi_\nu \tag{4.12}$$

Reading $a_l^{(in/out)}$ and ϕ_α as vector entries and substituting (4.11) into (4.10) and (4.12), yields:

$$i v_F \left(U \vec{a}^{(in)} - U^* \vec{a}^{(out)} \right) + W^\dagger \vec{\phi} = 0 \tag{4.13}$$

$$\varepsilon \vec{\phi} = H \vec{\phi} + \frac{1}{2} W \left(U \vec{a}^{(in)} + U^* \vec{a}^{(out)} \right) \tag{4.14}$$

Now we can eliminate the wavefunction inside the dot $\vec{\phi}$ in (4.13)-(4.14) and find $\vec{a}^{(out)}$, cf. (4.1). This yields the scattering matrix:

$$S(\varepsilon) = U^T \left[1 - i\pi\nu W^\dagger \left(H - \varepsilon \right)^{-1} W \right]^{-1} \left[1 + i\pi\nu W^\dagger \left(H + \varepsilon \right)^{-1} W \right] U \tag{4.15}$$

Here the density of states in the one dimensional leads $\nu = \frac{1}{2\pi v_F}$ has been introduced.

4.2. Finding the scattering matrix of the QPC

Since we want to investigate the coupling of the QD to the leads, it is convenient to seperate the S matrix of the total system into parts coming from the QPC and the QD. The following calculation is taken from [12]. If two leads with N channels each are connected to a scattering region, QPC a $2N \times 2N$ scattering matrix with time-reversal symmetry is assumed, so it has the structure:

$$\hat{S}_c = \begin{pmatrix} r_c & t_c^T \\ t_c & r_c' \end{pmatrix}$$

where r_c/t_c describes the reflection/transmission to the dot for waves coming from the leads and r'_c/t^T_c the reflection/transmission to the leads for waves coming from the dot. Let's denote the scattering matrix of the QD by S_0. The total scattering matrix must account for all pathes, on which an incoming electron can leave the dot:

$$S(\varepsilon) = r_c + t^T_c S_0(\varepsilon) t_c + t^T_c S_0(\varepsilon) r'_c S_0(\varepsilon) t_c + t^T_c S_0(\varepsilon) r'_c S_0(\varepsilon) r'_c S_0(\varepsilon) t_c + ...$$

The first term is direct reflection at the QPC and the remaining terms describe multiple reflections between the QPC and the QD before leaving the dot. This is a geometric series and thus $S(\varepsilon)$ can be written in the form:

$$S(\varepsilon) = r_c + t^T_c S_0(\varepsilon) \left[1 - r'_c S_0(\varepsilon)\right]^{-1} t_c \tag{4.16}$$

To split $S(\varepsilon)$ this way we first use a parametrization of W from [2]:

$$W = NVO\tilde{W} \quad . \tag{4.17}$$

Here N is a normalization constant, V is an orthogonal $M \times M$ matrix, O is a $M \times N$ projection matrix with $O_{mn} = \delta_{mn}$ and $\tilde{W}$ is a real $N \times N$ matrix, which describes the QPC. The normalization in [2] corresponds to a Lorentzian distribtution [12], so it must be adapted to fit the Gaussian distribution, which we use. It can be found by calculating the scattering matrix for $H = 1$ and assuming a ballistic QPC, which means that the reflection amplidtudes are zero. In this case, electrons with zero energy can only aquire a phase in the scattering process. Thus the scattering matrix must be the identity matrix multiplied with a phase factor $e^{i\Theta}$:

$$\begin{aligned} e^{i\Theta} &= -\left[1 - i\pi\nu W^\dagger W\right]^{-1} \left[1 + i\pi\nu W^\dagger W\right] \\ \Leftrightarrow W^\dagger W &= -\frac{1}{\pi\nu} \frac{\sin\Theta}{(1 - \cos\Theta)} \end{aligned}$$

Choosing $\Theta = \frac{3}{2}\pi$ to get an easy expression, yields for the nomalization factor $N = \frac{1}{\sqrt{\pi\nu}}$. Thus, (4.17) reduces to:

$$W = \frac{1}{\sqrt{\pi\nu}} VO\tilde{W} \quad . \tag{4.18}$$

Inserting (4.18) into (4.15) yields:

$$S(\varepsilon) = U \left[1 + i\tilde{W}^\dagger \tilde{H}(\varepsilon) \tilde{W}\right] \left[1 - i\tilde{W}^\dagger \tilde{H}(\varepsilon) \tilde{W}\right]^{-1} U^T \tag{4.19}$$

where $\tilde{H} = O^\dagger V^\dagger (H - \varepsilon)^{-1} VO$ was introduced. Since the distribution $P(H)$ is invariant under the orthogonal transformation, the rotation caused by V and V^T, does not change the distribution of the entries of H, one can argue that $\tilde{H}$ still describes only the random QD with the Hamiltonian taken from the WD-RMT. If

we put $\tilde{W} = U = 1$, than $S(\varepsilon) = S_0$:

$$S_0(\varepsilon) = \left[1 + i\tilde{H}(\varepsilon)\right]\left[1 - i\tilde{H}(\varepsilon)\right]^{-1} \Leftrightarrow \tilde{H} = i\left[1 - 2\left(1 + S_0(\varepsilon)\right)^{-1} S_0(\varepsilon)\right] \tag{4.20}$$

Inserting (4.20) into (4.19), one can find:

$$\begin{aligned} S(\varepsilon) &= U\frac{1 - \tilde{W}^\dagger\tilde{W}}{1 + \tilde{W}^\dagger\tilde{W}}U^T + \\ &+ \left(\tilde{W}\frac{2}{1 + \tilde{W}^\dagger\tilde{W}}U\right)_c^T S_0(\varepsilon)\left[1 + \tilde{W}\frac{1 - \tilde{W}^\dagger\tilde{W}}{1 + \tilde{W}^\dagger\tilde{W}}\tilde{W}^{-1}S_0(\varepsilon)\right]^{-1}\tilde{W}\frac{2}{1 + \tilde{W}^\dagger\tilde{W}}U \quad ; \end{aligned} \tag{4.21}$$

detailed calculations are presented in Appendix A. Comparing (4.16) and (4.21), we find the entries of $\hat{S}_c$:

$$r_c = U\frac{1 - \tilde{W}^\dagger\tilde{W}}{1 + \tilde{W}^\dagger\tilde{W}}U^T, \quad r_c' = -\tilde{W}\frac{1 - \tilde{W}^\dagger\tilde{W}}{1 + \tilde{W}^\dagger\tilde{W}}\tilde{W}^{-1}, \quad t_c = \tilde{W}\frac{2}{1 + \tilde{W}^\dagger\tilde{W}}U \quad . \tag{4.22}$$

If $\tilde{W}^\dagger\tilde{W} \approx 1$, the reflection amplitdues at the QPC are close to zero, corresponding to the almost ballistic coupling. For $\tilde{W}^\dagger\tilde{W} \approx 0$, the reflection amplitudes are close to -1, which corresponds to the almost closed QPC. This is a parametrization of a point like QPC, therefore the reflection amplitudes have to be in the interval $[-1, 0]$ due to Dirichlet boundary conditions for a point like scatterer. This restricts the elements of $\tilde{W}^\dagger\tilde{W}$ to the interval $[0, 1]$.

5. Numerical study of the effective Hamiltonian

5.1. Basic equations

In this thesis, we will study numerically a simple case with two leads attached to the QD. Furthermore, only one open channel per lead is assumed, so two broad energy levels are expected. Assuming that the QPCs are far away from each other, there is no mixing of channels in the reflection and transmission matrices of $\hat{S}_c$. Therefore, r_c, r_c' t_c and correspondingly $\tilde{W}$ are diagonal. With $U_{kl} = i\delta_{kl}$ the equations (4.22) read:

$$r_c = r_c' = -\frac{1-\tilde{W}\tilde{W}}{1+\tilde{W}\tilde{W}}, \quad t_c = i\tilde{W}\frac{2}{1+\tilde{W}\tilde{W}} \quad . \tag{5.1}$$

Matrix elements of $\tilde{W}^2$ can be found from the first equation of (5.1):

$$\tilde{W}_j^2 = \frac{1+r_j}{1-r_j} \quad . \tag{5.2}$$

Using (5.2) together with the parametrization for W as in equation (4.18), the effective Hamiltonian, (3.13), can be written as:

$$H_{eff} = H + iVO\tilde{W}\tilde{W}O^TV^T \quad . \tag{5.3}$$

The eigenvalues of the Hamiltonian does not change under the rotation by an orthogonal matrix and as explained before, the distribution of entries of H does also not change under such a rotation. Therefore, rotating (5.3) with the orthogonal matrix V yields the Hamiltonian, which will be used to calculate the energy levels and widths:

$$V^TH_{eff}V = H + iO\tilde{W}\tilde{W}O^T \quad . \tag{5.4}$$

This Hamiltonian will be diagonalized numerically with Matlab. The program code is presented in the Appendix B. Since $\tilde{W}$ is diagonal, $O\tilde{W}\tilde{W}O^T$ is $diag(\tilde{W}_1^2, \tilde{W}_2^2, 0, ..., 0)$, according to (5.2), and the rest being zero. The symmetric random matrix H in (5.4) will be initialisied by creating a random matrix and taking its upper triangular part, including the diagonal elements, and add the transposed of its upper triangular part, without the diagonal elements, to it. All entries are Gaussian distributed with mean value of zero and variance of one. The mean level spacing δ_l can be found for

every realization l of H from the real parts of the eigenvalues λ:

$$\Delta_l = \frac{\max\left[Re\left(\lambda\right)\right] - \min\left[Re\left(\lambda\right)\right]}{M} \quad . \tag{5.5}$$

The mean level widths Γ_l of every realization is calculated just as Δ_l, but with the imaginary parts of the eigenvalues. Averaging both quantities over many realizations of H gives the total mean level spacing Δ and the total mean level width Γ. Δ will be compared to Γ and is used as an unit for the level widths γ_i. Using the level widths for many realizations of the random matrix H, enables us to plot statistics.

5.2. Results of the calculations

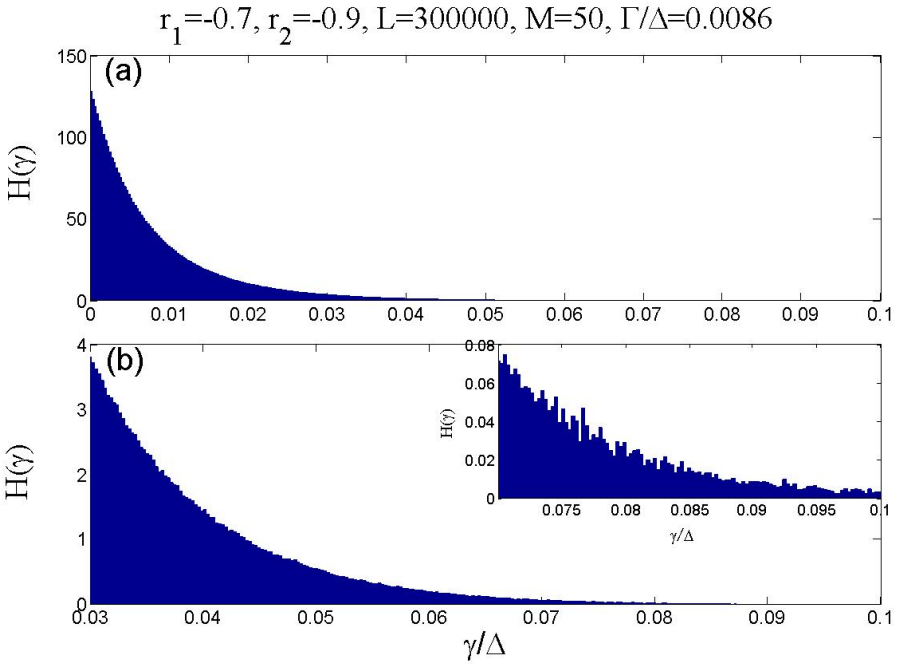

Figure 5.1.: Histogram for an almost closed QPC. (a) The distribution of all values of γ_i. (b) Zoomed in at higher values of γ.

First, the γ_i of $L = 10^5$ realizations are plotted in a histogram $H(\gamma)$, which is normalized so $\int H(\gamma)d\gamma = 1$. For an almost closed QPC, where r_1 and r_2 are close to -1, the result is shown in Figure 5.1. The distribution 5.1(a) can be fitted quite well by an exponential decay, with the most probable level width at zero. Since we are interested in the broad energy levels, the same distribution zoomed in at higher values of γ is shown in Figure 5.1(b). At higher values, the distribution still looks like an exponential decay and there is no behaviour indicating the existance of stable broad energy levels. Due to the long tail of the distribution, fluctuations of the broad energy levels are large. Since $\frac{\Gamma}{\Delta} \approx 0.008 \ll 1$, this behaviour is expected

[8].The same plots for an almost ballistic QPC,where r_1 and r_2 are close to 0, are shown in Figure 5.1. The behaviour is qualitativly the same as for the almost closed QPC. The distribution looks like an exponential decay, but is flatter than in the almost closed QPC, so there is a trend to broader energy levels. But there is still no peak at higher level widths, which would indicate a scale seperation. $\frac{\Gamma}{\Delta} \approx 0.051$ is still much smaller than one. The trend is a higher ratio $\frac{\Gamma}{\Delta}$ for reflection amplitudes closer to zero. For $r_j = 0$, $\frac{\Gamma}{\Delta} \approx 0.075$ is the maximal value, which can be reached in this model. This is still far from the regime $\frac{\Gamma}{\Delta} \geq 1$, which was observed for the existance of the broad energy levels in [8].

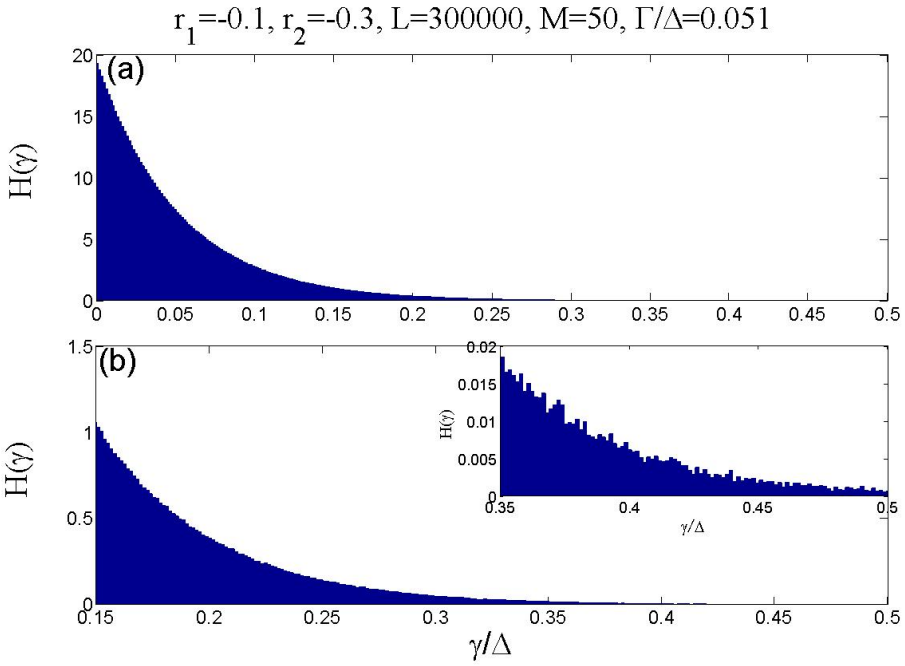

Figure 5.2.: Histogram for an almost ballistic QPC. (a) The distribution of all values of γ_i. (b) Zoomed in at higher values of γ.

Since there can still be a scale seperation in this model, which is just not visible in the statistics of many realizations of disorder in the QD due to strong fluctuations, γ_i of several, randomly choosen, realizations are plotted in Figure 5.3 and 5.4. In panel (a) of each Figure, a single realization of γ_i is plotted. After looking at many randomly picked realizations, both were chosen to reflect the typical pictures. For the almost closed as well as for the almost ballistic QPC, there is no scale seperation at all. In rare cases, there are gaps in between the level widths, but that is due to the fluctuations arising from the random matrix and do not reflect a stable distribution of energy widths. In panel (b) of 5.3 and 5.4, 10 realizations of γ_i are plotted. The fluctuations of the two highest energy levels overlap with the fluctuations of the narrow energy levels, so no gap in the level widths can be seen. The other parameter which can be changed in this model is M, the number of energy levels inside the

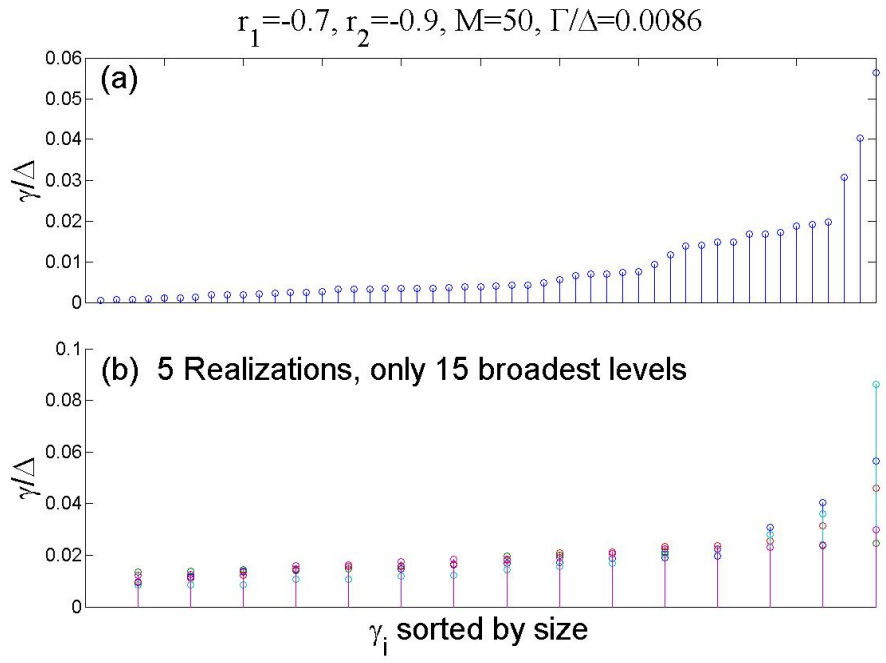

Figure 5.3.: Randomly choosen realizations of disorder for the almost closed QPC. (a) γ_i of a single realization, which was found to be typical in this configuration. (b) γ_i of 5 different realizations.

QD. As M decreases, it scales the total mean level width Γ, but does not change the qualitative behaviour of the system, down to $M = 5$. At this point $\frac{\Gamma}{\Delta} \approx 0.25$ and there is still no gap seperating broad and narrow energy levels. Increasing M reduces the ratio $\frac{\Gamma}{\Delta}$ even further and does not bear new results.

In this model the regime of the broad energy levels could not be reached, since $\frac{\Gamma}{\Delta} \ll 1$. So far r_j are bounded to $r_j \in [-1, 0]$, which reflects a coupling of $\tilde{W}_j^2 \in [0, 1]$ (cf. Eq.(5.2)). Relaxing this constriction to $r_j \in [-1, 1]$ reflects an arbitrary coupling with no bounds. The only possibility to enter the regime $\frac{\Delta}{\Gamma} \geq 1$ is using stronger couplings $\tilde{W}^2$ and therefore violating the constrictions of the point like scatterer. Using $r_j > 0$ to see whether broad energy levels exist for stronger couplings yields the results in Figure 5.5. Additionally peaks can be observed in the statistics as the regime $\frac{\Gamma}{\Delta} \approx 1$ is entered, so broad energy levels mathematically exist in the RMT model and an alternative description of the QPC could help.

5.3. Comparing the results to a constant δ model

In this section we reproduce numerical results obtained in [8] for the model described in the introduction and compare them with our findings for the RMT-based model. The structure of the effective Hamiltonian in [8] is:

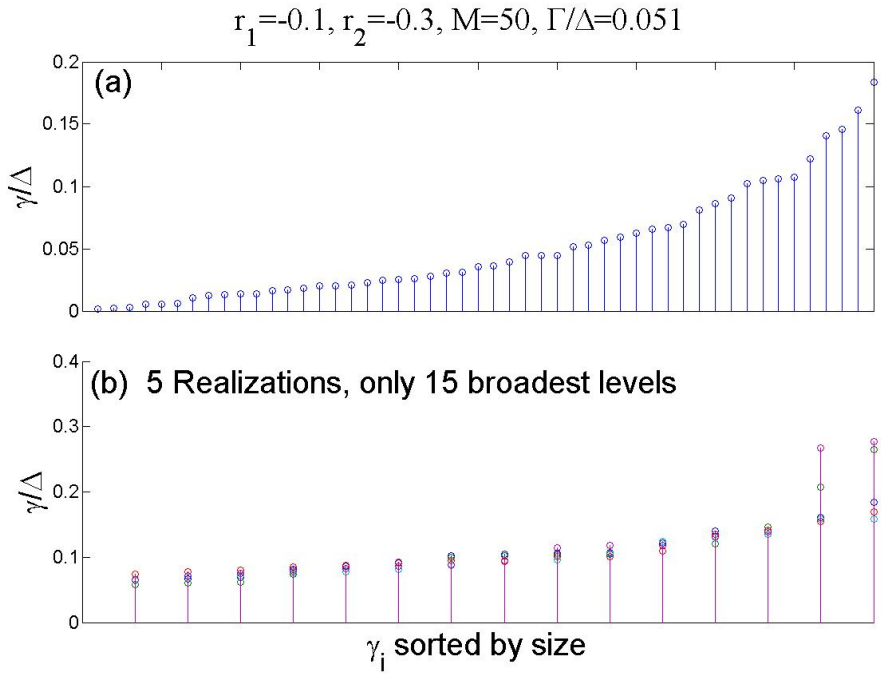

Figure 5.4.: Randomly choosen realizations of disorder for the almost ballistic QPC. (a) γ_i of a single realization, which was found to be typical in this configuration. (b) γ_i of 5 different realizations.

$$H_{eff,c} = h + i\pi\nu t t^T \quad . \tag{5.6}$$

t is the $M \times N_{ch}$ coupling matrix from (1.7) and h is a $M \times M$ diagonal matrix with the entries ε_i from (1.5). The levelspacing is constant and equal the mean level spacing from the random matrix model, so the results are comparable: $\Delta = 0.5322$ for $M = 50$. The coupling matrix t will be parametrized as W before:

$$t = \frac{1}{\sqrt{\pi\nu}} V O \tilde{t} \quad . \tag{5.7}$$

Here $\tilde{t}$ is a diagonal $N_{ch} \times N_{ch}$ matrix and V is used to get a full coupling matrix.

$$\rightarrow H_{eff,c} = h + iVO\tilde{t}\tilde{t}^T O^T V^T \quad . \tag{5.8}$$

The mean level width Γ is given by:

$$\Gamma = \frac{\pi\nu}{M} \sum_{\alpha j} t_{\alpha j}^2 = \frac{\pi\nu}{M} Tr\left[tt^T\right] = \frac{1}{M} Tr\left[O\tilde{t}\tilde{t}O^T\right] \tag{5.9}$$

Assuming two leads with one channel in each lead, $\tilde{t}$ can be parametrized by a reflection amplitude r_j, Eq. (5.2) after substitutiong $\tilde{t}$ for $\tilde{W}$. This way the coupling

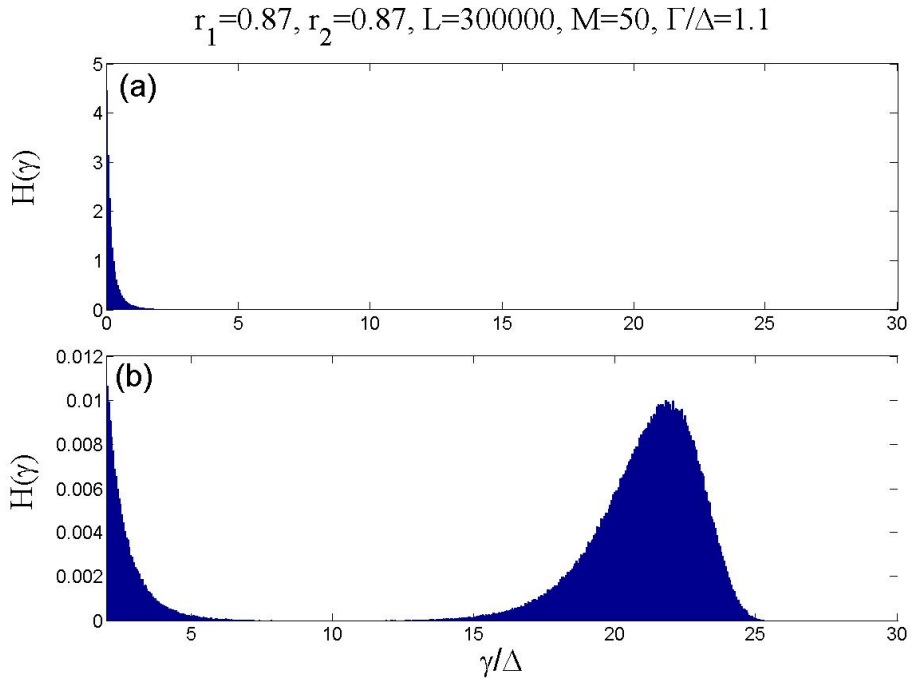

Figure 5.5.: Histogram for an almost ballistic QPC with positice reflection amplitudes. (a) All values. (b) Zoomed in at higher γ.

strengths can be compared to the previous calculations. Since t has no restrictions in [8], it will be taken from the interval $[-1, 1]$. V is chosen as the symmetric eigenvector matrix for second difference matrix (taken from the help catalogue of Matlab) to get an easy way of getting an orthogonal matrix of any size. The program code can be found in appendix C. The results are summarized in Figure 5.6. Firstly, we study negative $r_{1,2}$ similar to the RMT model for the almost ballistic QPC, see panel (a). In this case $\frac{\Gamma}{\Delta} << 1$ there is no gap between broad and narrow energy levels. For positive reflection amplitudes r_j, a seperation of scales can be observed at at $\frac{\Gamma}{\Delta} \approx 0.25$, see Figure 5.6(b)-(d). This is in a qualitative agreement with [8]. So neither in the diagonal model nor in the RMT model do broad energy levels exist for $r_j \in [-1, 0]$, while both models show a gap for $r_j in [0, 1]$.

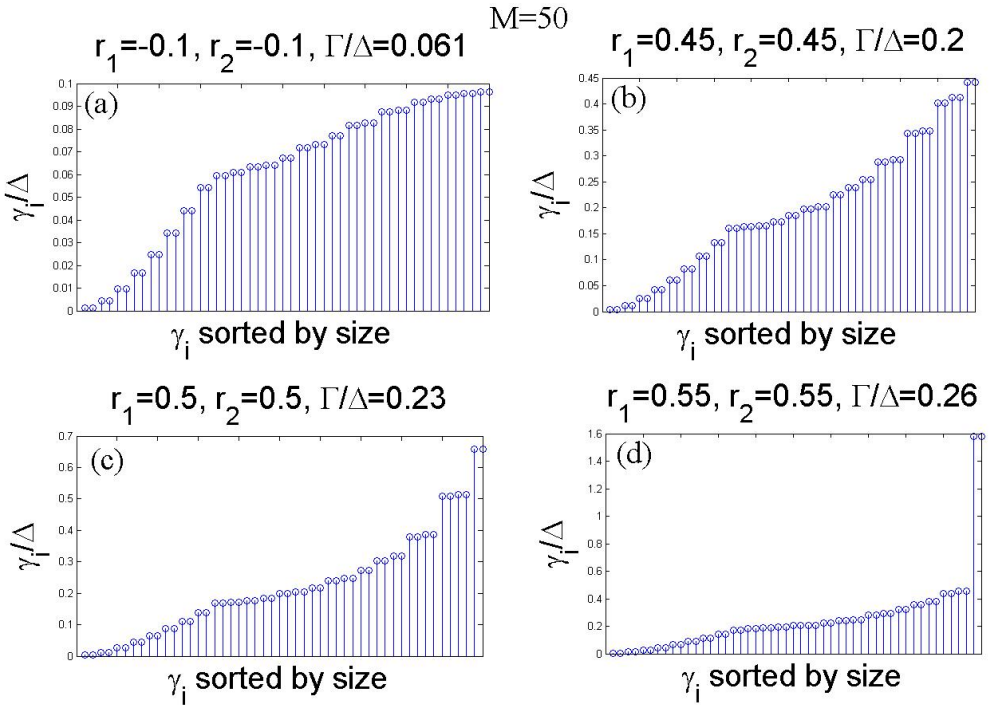

Figure 5.6.: Level widths of a diagonal Hamiltonian for the dot with constant level spacing. (a) Negative reflection amplitdues as in the previous model. There is no gap between broad and narrow energy levels. (b)-(d) A gap emerges and becomes clearly visible at positive r_j, where $\Gamma \to \Delta$.

6. Alternative description of the QPC

In the previous chapter it was shown that broad energy levels do not exist within the restriction of $r_j \in [-1, 0]$. This restriction origins at the Dirichlet boundary conditions for the point like QPC. Therefore a different description of the QPC, with different boundary conditions, is needed. A possible solution is a QPC with a finite width of boundaries, which must be described by their own S-matrices without restrictions assumed for point like scatterers.

6.1. Composing S_c from two scatterers

To parametrize the QPC, a left and a right boundary of the QPC is defined. The boundaries can be represented by the two scattering matrices $S_{L/R}$, which are unitary and assumed to be time-reversal ($S_{L/R} = S_{L/R}^T$) and left-right symmetric ($S_{L/R} = \tau_2 S_{L/R} \tau_2$, with τ_2 being the Pauli matrix). Furthermore, no mixing of channels is assumed, so the reflection and transmission matrices in the scattering matrix are diagonal. The unitarity condition for a S-matrix with diagonal entries yields an equivalent and independent set of equations for every channel, so only a one channel problem has to be solved. Therefore, a one channel problem will be considered from here on and channel indices will be omitted. From the general parametrization of a 2×2 unitary matrix

$$S = e^{i\phi} \begin{pmatrix} \cos(\alpha) e^{i\nu} & i \sin(\alpha) e^{i\mu} \\ i \sin(\alpha) e^{-i\mu} & \cos(\alpha) e^{-i\nu} \end{pmatrix}$$

the conditions for the imposed symmetries can be found. Time-reversal symmetrie yields: $e^{i\phi} i \sin(\alpha) e^{i\mu} = e^{i\phi} i \sin(\alpha) e^{-i\mu} \Leftrightarrow \mu = 0$ and left-right symmetry yields: $e^{i\phi} \cos(\alpha) e^{i\nu} = e^{i\phi} \cos(\alpha) e^{-i\nu} \Leftrightarrow \nu = 0$. Introducing $r_{L/R} = \cos(\alpha_{L/R})$ and $t_{L/R} = \sin(\alpha_{L/R})$ so $r_{L/R}^2 + t_{L/R}^2 = 1$ results in:

$$S_{L/R} = e^{i\phi_{L/R}} \begin{pmatrix} r_{L/R} & i t_{L/R} \\ i t_{L/R} & r_{L/R} \end{pmatrix} \quad . \tag{6.1}$$

In the most general case S_c matrix has the structure as stated in (1.3), but it can still be multiplied by a global phase factor $e^{i\Phi}$ without violating the unitarity condition:

$$S_c = e^{i\Phi} \begin{pmatrix} r_c & t_c' \\ t_c & r_c' \end{pmatrix} \quad .$$

r_c/t_c and r'_c/t'_c are matrices describing reflection/transmission from the left and the right respectively. To compose S_c from $S_{L/R}$, all paths that traverse both boundaries of the QPC are summed up in t_c/t'_c and all paths that do not traverse both boundaries yield r_c/r'_c. Figure 6.1 illustrates this procedure.

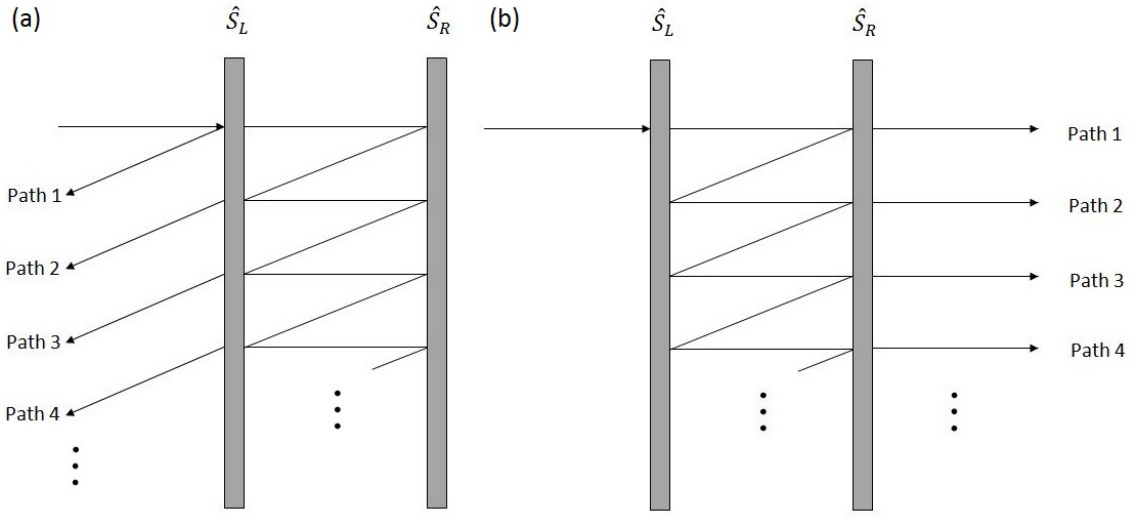

Figure 6.1.: (a) Paths adding up to the reflection of the QPC. (b) Paths adding up to the transmission of the QPC.

Because of this construction, the assumption of non-mixing channels in $S_{L/R}$ transfers to S_c. The entries of S_c read:

$$\begin{aligned} r_c &= e^{i\phi_L} r_L - e^{i(2\phi_L+\phi_R)} t_L r_R t_L - e^{i(3\phi_L+2\phi_R)} t_L r_R r_L r_R t_L - ... \\ \rightarrow r_c &= e^{i\phi_L} r_L - \frac{e^{i(2\phi_L+\phi_R)} t_L^2 r_R}{1 - e^{i(\phi_L+\phi_R)} r_R r_L} = e^{i\phi_L} \frac{r_L - e^{i(\phi_L+\phi_R)} r_R}{1 - e^{i(\phi_L+\phi_R)} r_R r_L} \end{aligned} \tag{6.2}$$

$$\begin{aligned} t_c &= -e^{i(\phi_L+\phi_R)} t_L t_R - e^{i(2\phi_L+2\phi_R)} t_L r_R r_L t_R - ... \\ \rightarrow t_c &= -\frac{e^{i(\phi_L+\phi_R)} t_L t_R}{1 - e^{i(\phi_L+\phi_R)} r_R r_L} \end{aligned} \tag{6.3}$$

r'_c and t'_c follow by exchanging L and R in the indices. It follows that $t_c = t'_c$, so the time-reversal symmetry also transfers from $S_{L/R}$ to S_c. r'_c reads:

$$r'_c = e^{i\phi_R} \frac{r_R - e^{i(\phi_L+\phi_R)} r_L}{1 - e^{i(\phi_L+\phi_R)} r_R r_L} \tag{6.4}$$

So whether the entries of S_c are real or complex depends on the global phases ϕ_L and ϕ_R. In this case the unitarity condition $S_c S_c^\dagger = 1$, yields:

$$e^{i\Phi} \begin{pmatrix} r_c & t_c \\ t_c & r'_c \end{pmatrix} e^{-i\Phi} \begin{pmatrix} r_c^* & t_c^* \\ t_c^* & r'^*_c \end{pmatrix} = \begin{pmatrix} r_c r_c^* + t_c t_c^* & r_c t_c^* + t_c r'^*_c \\ t_c r_c^* + r'_c t_c^* & t_c t_c^* + r'_c r'^*_c \end{pmatrix} = \begin{pmatrix} 1 & 0 \\ 0 & 1 \end{pmatrix} \quad .$$

This is equivalent to the three independent equations:

$$|r_c|^2 + |t_c|^2 = 1 \tag{6.5}$$

$$t_c r_c^* + r_c' t_c^* = 0 \tag{6.6}$$

$$|r_c'|^2 + |t_c|^2 = 1 \tag{6.7}$$

With r_c, r_c' and t_c it can be validated if the constructed S_c can be unitary:

$$|r_c|^2 = |r_c'|^2 = \frac{r_L^2 + r_R^2 - 2\cos(\phi_L + \phi_R) r_L r_R}{1 + r_L^2 r_R^2 - 2\cos(\phi_L + \phi_R) r_L r_R}$$

$$|t_c|^2 = \frac{t_L^2 t_R^2}{1 + r_L^2 r_R^2 - 2\cos(\phi_L + \phi_R) r_L r_R} = \frac{1 - r_L^2 - r_R^2 + r_L^2 r_R^2}{1 + r_L^2 r_R^2 - 2\cos(\phi_L + \phi_R) r_L r_R}$$

Therefore (6.5) and (6.7) are fulfilled. (6.6) reads:

$$-\frac{e^{i(\phi_L+\phi_R)} t_L t_R e^{-i\phi_L}(r_L - e^{-i(\phi_L+\phi_R)} r_R) + e^{-i(\phi_L+\phi_R)} t_L t_R e^{i\phi_R}(r_R - e^{i(\phi_L+\phi_R)} r_L)}{(1 - e^{i(\phi_L+\phi_R)} r_R r_L)(1 - e^{-i(\phi_L+\phi_R)} r_R r_L)} = 0$$

By omitting the trivial cases with $r_L, r_R, t_L, t_R = 0, 1$ it follows:

$$\begin{aligned} &\Rightarrow e^{i\phi_R}(r_L - e^{-i(\phi_L+\phi_R)} r_R) + r^{-i\phi_L}(r_R - e^{i(\phi_L+\phi_R)} r_L) = 0 \\ &\Leftrightarrow e^{i\phi_R} r_L - e^{-i\phi_L} r_R + e^{-i\phi_L} r_R - e^{i\phi_R} r_L = 0 \end{aligned}$$

This is true, so S_c is unitary by construction. Since the equations (5.1) must still be fullfilled in this picture, the condition $r_c = r_c'$, which is left-right symmetry, must be imposed on S_c. Furthermore, the value for the global phase can be deduced as either $\Phi_1 = \frac{\pi}{2}$ or $\Phi_2 = \frac{3\pi}{2}$ by comparison. Implying this on (6.2) and (6.4) yields:

$$\begin{aligned} &\rightarrow e^{i\phi_L} \frac{r_L - e^{i(\phi_L+\phi_R)} r_R}{1 - e^{i(\phi_L+\phi_R)} r_R r_L} = e^{i\phi_R} \frac{r_R - e^{i(\phi_L+\phi_R)} r_L}{1 - e^{i(\phi_L+\phi_R)} r_R r_L} \\ &\Leftrightarrow e^{i\phi_L} r_L - e^{i(2\phi_L+\phi_R)} r_R = e^{i\phi_R} r_R - e^{i(\phi_L+2\phi_R)} r_L \\ &\Leftrightarrow (1 + e^{i2\phi_R}) e^{i\phi_L} r_L = (1 + e^{i2\phi_L}) e^{i\phi_R} r_R \end{aligned}$$

For this to be true for all $r_{L/R}$, it follows: $\phi_L = \phi_R = \frac{\pi}{2}$. The total reflection and transmission entries read:

$$r_t = e^{i\Phi_{1/2}} r_c = e^{i\Phi_{1/2}} r_c' = \mp \frac{r_L + r_R}{1 + r_R r_L} \tag{6.8}$$

$$t_t e^{i\Phi_{1/2}} t_c = \pm i \frac{t_L t_R}{1 + r_R r_L} \tag{6.9}$$

6.2. How to express $\tilde{W}$ in terms of $r_{L,R}$

By comparing (5.1) to (6.8) and (6.9), $\tilde{W}$ can be expressed in terms of $r_{L/R}$. Assuming $\tilde{W}$ being diagonal, this yields an equivalent and independent set of equations for each channel. Therefore channel indices will be dropped again and only an one channel problem has to be solved: $\tilde{W}_{ii} \equiv \tilde{W}$. The equations read:

$$\frac{1-\tilde{W}^2}{1+\tilde{W}^2} = \pm\frac{r_L + r_R}{1 + r_R r_L} \tag{6.10}$$

$$\frac{2\tilde{W}}{1+\tilde{W}^2} = \pm\frac{t_L t_R}{1 + r_R r_L} \quad . \tag{6.11}$$

The solution to (6.10) and (6.12) with $t_{L/R}^2 = 1 - r_{L/R}^2 = (1 - r_{L/R})(1 + r_{L/R})$, reads:

$$\tilde{W}_{1/2} = \pm\sqrt{\frac{(1 \mp r_R)(1 \mp r_L)}{(1 \pm r_R)(1 \pm r_L)}} = \pm\frac{1 \mp r_R}{t_R} \quad \frac{1 \mp r_L}{t_L} \quad . \tag{6.12}$$

The upper sign is true for $\Phi_1 = \frac{\pi}{2}$ and the lower for $\Phi_2 = \frac{3\pi}{2}$. This parametrization of the QPC has two degrees of freedom in each channel, while the point like description only had one degree of freedom. In this parametrization the Direchlet boundary conditions of the point like QPC are replaced by the unitarity condition of the scattering matrix S_c. Therefore, there is no restriction on r_j in this parametrization and $\tilde{W}\tilde{W}^\dagger$ is now arbitrary. For $r \to 0$, $\tilde{W}\tilde{W}^\dagger \approx 0$ and for $t_c \to 0$, $\tilde{W}\tilde{W}^\dagger \to \infty$.

7. Conclusion

We have studied a RMT model for a QD coupled to noninteracting leads via QPCs to see whether broad energy levels also emerge in a certain regime. These broad levels are needed in [8] to describe the transport effect of phase lapses. A numerical approach was used to find the distribution function of the level widths. The main result is that generically, the broad energy levels can not be observed with a point like description of the QPC with the Dirichlet boundary conditions at the interfaces [2]. The Dirichlet boundary condition of a point like QPC, restricts the coupling amplitudes, so that it is not possible to reach the regime $\frac{\Gamma}{\Delta} \approx 1$. This holds true for the RMT model and for the model of the regular QD, used previously in [8]. The emergence of the broad energy levels can only be observed in both models if the restriction on the reflection amplitude of the QPC is removed. This can be done if we assume that the interfaces of the QPC are extended , so each should be described by the S-matrix, but the Kirchhof's law does not apply. We have suggested a new description of the QPC, which corresponds to such systems. This way the restriction on the reflection amplitudes can be lifted and broad energy levels exist in both models.

A. Derivation of equation (4.21)

For this calculation two identities are needed:

$$(I) : (1+PQ)^{-1} P = P (1+QP)^{-1}$$
$$(II) : (1+P)^{-1} = 1 - (1+P)^{-1} P$$

Proof:

$$(I) : P(1+QP) = P + PQP = (1+PQ)P$$
$$\Leftrightarrow (1+PQ)^{-1} P (1+QP)(1+QP)^{-1} = (1+PQ)^{-1}(1+PQ) P (1+QP)^{-1}$$
$$\Leftrightarrow (1+PQ)^{-1} P = P (1+QP)^{-1}$$

For shorter notation r_c, r'_c and t_c, as stated in (4.22), will be substituted as soon as possible.

$$S(\varepsilon) = U \left[1 - \tilde{W}^\dagger \left[1 - 2(1+S_0(\varepsilon))^{-1} S_0(\varepsilon)\right] \tilde{W}\right] \times$$
$$\times \left[1 + \tilde{W}^\dagger \left[1 - 2(1+S_0(\varepsilon))^{-1} S_0(\varepsilon)\right] \tilde{W}\right]^{-1} U^T =$$
$$= U \left[\underbrace{\left(1 - \tilde{W}^\dagger \tilde{W}\right)}_{=:N_-} + 2\tilde{W}^\dagger (1+S_0(\varepsilon))^{-1} S_0(\varepsilon) \tilde{W} \right] \times$$
$$\times \left[\underbrace{\left(1 + \tilde{W}^\dagger \tilde{W}\right)}_{=:N_+} - 2\tilde{W}^\dagger (1+S_0(\varepsilon))^{-1} S_0(\varepsilon) \tilde{W} \right]^{-1} U^T =$$
$$= U \left[N_- + 2\tilde{W}^\dagger (1+S_0(\varepsilon))^{-1} S_0(\varepsilon) \tilde{W}\right] N_+^{-1} \times$$
$$\times \left[1 - \underbrace{2\tilde{W}^\dagger (1+S_0(\varepsilon))^{-1} S_0(\varepsilon) \tilde{W} N_+^{-1}}_{=:X}\right]^{-1} U^T =$$
$$= U \left\{ N_- N_+^{-1} \underbrace{[1-X]^{-1}}_{\text{use } (II)} + X [1-X]^{-1} \right\} U^T =$$

$$= U\left\{N_- N_+^{-1}\left(1+\left[1-X\right]^{-1}X\right)+X\left(1-X\right)^{-1}\right\}U^T =$$

$$= U\left\{N_- N_+^{-1}+\left(N_- N_+^{-1}+1\right)\left[1-X\right]^{-1}X\right\}U^T =$$

$$= \underbrace{UN_-N_+^{-1}U^T}_{=r_c} + U^T \underbrace{\left(N_- + N_+\right)}_{=2} N_+^{-1} \underbrace{\left[1-2\tilde{W}^\dagger\left(1+S_0(\varepsilon)\right)^{-1}S_0(\varepsilon)\tilde{W}N_+^{-1}\right]^{-1}\tilde{W}^\dagger}_{\text{use } (I) \text{with } P=\tilde{W}^\dagger} \times$$

$$\times \left(1+S_0(\varepsilon)\right)^{-1}S_0(\varepsilon)\underbrace{\tilde{W}2N_+^{-1}U}_{=t_c} =$$

$$= r_c + \underbrace{U^T 2N_+^{-1}\tilde{W}^\dagger}_{=t_c^T}\left[1-2\left(1+S_0(\varepsilon)\right)^{-1}S_0(\varepsilon)\tilde{W}N_+^{-1}\tilde{W}^\dagger\right]^{-1}\left(1+S_0(\varepsilon)\right)^{-1}S_0(\varepsilon)t_c =$$

$$= r_c + t_c^T\left[1+S_0(\varepsilon)-2S_0(\varepsilon)\tilde{W}N_+^{-1}\tilde{W}^\dagger\right]^{-1}S_0(\varepsilon)t_c =$$

$$= r_c + t_c^T\left[1+S_0(\varepsilon)\left(1-2\tilde{W}N_+^{-1}\tilde{W}^\dagger\right)\right]^{-1}S_0(\varepsilon)t_c =$$

$$\overset{(I)}{=} r_c + t_c^T S_0(\varepsilon)\left[1+\left(\tilde{W}N_+N_+^{-1}\tilde{W}^{-1}-2\tilde{W}N_+^{-1}\tilde{W}^\dagger\tilde{W}\tilde{W}^{-1}\right)S_0(\varepsilon)\right]^{-1}t_c =$$

$$= r_c + t_c^T S_0(\varepsilon)\left[1+\tilde{W}\left(N_+N_+^{-1}-2N_+^{-1}\tilde{W}^\dagger\tilde{W}\right)\tilde{W}^{-1}S_0(\varepsilon)\right]^{-1}t_c =$$

$$= r_c + t_c^T S_0(\varepsilon)\left[1+\tilde{W}\underbrace{\left(N_+-2\tilde{W}^\dagger\tilde{W}\right)}_{=N_-}N_+^{-1}\tilde{W}^{-1}S_0(\varepsilon)\right]^{-1}t_c =$$

$$= r_c + t_c^T S_0(\varepsilon)\left[1-\underbrace{\left(-\tilde{W}N_-N_+^{-1}\tilde{W}^{-1}\right)}_{=r_c'}S_0(\varepsilon)\right]^{-1}t_c =$$

$$= r_c + t_c^T S_0(\varepsilon)\left[1-r_c' S_0(\varepsilon)\right]^{-1}t_c$$

B. Code for the random matrix Hamiltonian

```
%number of channels in the dot
M = 50;

%number of intervals for the historgram of all eigenvalues
res = 500;

%number of disorder realizations
L = 10000;

%number of randomly picked realizations plottet in one figure
nall = 5;

%number of randomly picked realizations plottet in distinct figures
nsin = 5;

%refelction amplitudes of the QPC
r = [-0.1  -0.3];

%calculate selfenergy part
d = size(r);
W2 = zeros(M);
for m=1:d(2)
     W2(m,m) = (1+r(m))/(1-r(m));
end

%calculate imagniary parts of the eigenvalues in units of mean levelspacing for all realizations
data = zeros(L*M,1);
delta = 0;
gamma = 0;
for k=1:L
     A = normrnd(0,1,M,M);
     H = triu(A)+(triu(A,1).')+1i*W2;
     lambda = (eig(H)).';
     gamma = gamma + imag(sum(lambda))/M;
     data((k-1)*M+1:k*M) = imag(lambda);
     delta = delta + (max(real(lambda))-min(real(lambda)))/M;
end

gamma = gamma/L;
delta = delta/L;
data_mls = data/delta;
[n,x]=hist(data_mls,res);
delta_x = x(2) - x(1);

%plot statistic of all realisations
figure
bar(x,n/sum(n*delta_x),'hist');
set(gca,'FontSize',30);
title(sprintf('r_1=%g, r_2=%g, L=%g, M=%g, \\Gamma/\\Delta=%0.2g',r(1),r(2),L,M,gamma/delta));
```

```
50 ylabel('normalized number of occurences');
51 xlabel('\gamma/\Delta');
52 legend(sprintf('bar width=%g',delta_x));
53
54
55 %plot single randomly taken realisations in different plots
56 rsin = randi(L,nsin,1);
57
58 for z=1:nsin
59     figure
60     pic = sort(data_mls(M*rsin(z)-M+1:M*rsin(z)));
61     stem(pic);
62     set(gca,'FontSize',30);
63     title(sprintf('r_1=%g, r_2=%g, M=%g, \\Gamma/\\Delta=%0.2g',r(1),r(2),M,gamma↩
           /delta));
64     xlabel('\gamma sorted by size');
65     ylabel('\gamma/\Delta');
66     set(gca, 'XTickLabelMode', 'manual', 'XTickLabel', []);
67 end
68
69 %plot randomly taken realisations into one plot
70 rall = randi(L,nall,1);
71
72 figure
73 set(gca,'FontSize',30);
74 title(sprintf('r_1=%g, r_2=%g, M=%g, \\Gamma/\\Delta=%0.2g, %g Realizations',r(1)↩
       ,r(2),M,gamma/delta,nall));
75 xlabel('\gamma sorted by size');
76 ylabel('\gamma/\Delta');
77 set(gca, 'XTickLabelMode', 'manual', 'XTickLabel', []);
78
79 hold all
80
81 for zall=1:nall
82     pic = sort(data_mls(M*rall(zall)-M+1:M*rall(zall)));
83     stem(pic);
84 end
```

C. Code for the constant level spacing Hamiltonian

```
%number of channels in the dot
M = 50;

%levelspacing in the dot
delta = 0.5322;

%refelction amplitudes of the QPC
r = [-0.7  -0.9];

%orthogonal matrix
V = gallery('orthog',M,1);

%diagonal hamiltonian for the dot
H = zeros(M);
for q=1:M
    H(q,q) = q*delta;
end

%selfenergy part
t2 = zeros(M,M);
gamma=0;
d = size(r);
for m=1:d(2)
    t2(m,m) = (1+r(m))/(1-r(m));
    gamma = gamma + t2(m,m);
end
gamma = gamma/M;

E = 1i*V*t2*(V.');

%eigenvalues
Heff = H + E;
lambda = eig(Heff);

%plot level widths
figure
stem(sort(imag(lambda)/delta));
title(sprintf('r_1=%g, r_2=%g, M=%g, \\Gamma/\\Delta=%0.2g',r(1),r(2),M,gamma/↩
    delta),'FontSize',30);
xlabel('\gamma_i sorted by size','FontSize',30);
ylabel('\gamma_i/\delta','FontSize',30);
set(gca, 'XTickLabelMode', 'manual', 'XTickLabel', []);
```

Bibliography

[1] J. Feldmann, lecture notes on "Advanced Solid State Physics", LMU (2013/14).

[2] I.L. Aleiner, P.W. Brouwer, L.I. Glazman, Physics Reports **358** (2002), pp. 309-440.

[3] J. von Delft, lecture notes on "Mesoscopics", LMU (2013).

[4] Y. Yacoby *et al.*, Phys. Rev. Lett. **74**, 4047 (1995).

[5] S. Datta, *Electronic Transport in Mesoscopic Systems* (Cambridge University Press, New York, 1995).

[6] R. Schuster *et al.*, Nature (London) **385**, 417 (1997).

[7] M. Avinun-Khalish *et al.*, Nature (London) **436**, 529 (2005).

[8] C. Karrasch, T. Hecht, A. Weichselbaum, Y. Oreg, J. von Delft, V. Meden, Phys. Rev. Lett **98**, 186802 (2007).

[9] Yuli V. Nazarov, Yaroslav M. Blanter, *Quantum Transport* (Cambridge University Press, New York, 2009).

[10] T. Hecht, A. Weichselbaum, Y. Oreg, J. von Delft, Phys. Rev. B **80**, 115330 (2009).

[11] I.L.Kurland, I.L. Aleiner, B.L. Altshuler, Phys. Rev. B **62**, 14886 (2000).

[12] P.W. Brouwer, Phys. Rev. B **51**, 16878 (1995).

[13] U. Fano, Phys. Rev. **124**, 1866 (1961).

[14] M.L. Mehta, *Random Matrices* (Elsevier Academic Press, Amsterdam, 2004).

[15] A.L. Fetter, J.D. Walecka, *Quantum Theory of Many-Particle Systems* (Dover Publications, New York, 1971).

[16] C. Karrasch, T. Hecht, A. Weichselbaum, Y. Oreg, J. von Delft, V. Meden, New Journal pf Physics **9**, (2007) 123.

[17] A. Altland, B. Simons, *Condensed Matter Field Theory* (Cambridge University Press, New York, 2006).

Acknowledgements

I want to thank Dr. Oleg Yevtushenko for introducing me to the field of electron transport in mesoscopic systems and giving me the chance to work on this subject. He guided me patiently in this thesis with explanations and discussions. Furthermore his helping hand in correcting mistakes and proof reading my thesis was very valuable and I am very grateful for that.
I also want to thank Prof. Jan von Delft for looking into the problem when we got stuck.

Statutory Declaration

I declare on oath that I completed this work on my own and that information which has been directly or indirectly taken from other sources has been noted as such. Neither this, nor a similar work, has been published or presented to an examination committee.

Munich, December 20, 2013

Place, Date

signature